Geophysical Journal International

Geophys. J. Int. (2022) **231,** 1573–1590
Advance Access publication 2022 July 23
GJI Seismology

https://doi.org/10.1093/gji/ggac268

Source scaling comparison and validation in Central Italy: data intensive direct *S* waves versus the sparse data coda envelope methodology

Paola Morasca [1], Dino Bindi [2], Kevin Mayeda,[3] Jorge Roman-Nieves,[3] Justin Barno,[4] William R. Walter [4] and Daniele Spallarossa[5]

[1] *Istituto Nazionale di Geofisica e Vulcanologia, INGV, Milan, Italy. E-mail: paola.morasca@ingv.it*
[2] *Deutsches GeoForschungsZentrum GFZ, Potsdam, Germany*
[3] *Air Force Technical Applications Center, AFTAC, Patrick Air Force Base, USA*
[4] *Lawrence Livermore National Laboratory, LLNL, CA, USA*
[5] *Dipartimento di Scienze della Terra dell'Ambiente e della Vita, Università di Genova, UNIGE, Genoa, Italy*

Accepted 2022 July 20. Received 2022 May 23; in original form 2021 November 26

SUMMARY

Robustness of source parameter estimates is a fundamental issue in understanding the relationships between small and large events; however, it is difficult to assess how much of the variability of the source parameters can be attributed to the physical source characteristics or to the uncertainties of the methods and data used to estimate the values. In this study, we apply the coda method by Mayeda *et al.* using the coda calibration tool (CCT), a freely available Java-based code (https://github.com/LLNL/coda-calibration-tool) to obtain a regional calibration for Central Italy for estimating stable source parameters. We demonstrate the power of the coda technique in this region and show that it provides the same robustness in source parameter estimation as a data-driven methodology [generalized inversion technique (GIT)], but with much fewer calibration events and stations. The Central Italy region is ideal for both GIT and coda approaches as it is characterized by high-quality data, including recent well-recorded seismic sequences such as L'Aquila (2009) and Amatrice–Norcia–Visso (2016–2017). This allows us to apply data-driven methods such as GIT and coda-based methods that require few, but high-quality data. The data set for GIT analysis includes ∼5000 earthquakes and more than 600 stations, while for coda analysis we used a small subset of 39 events spanning $3.5 < M_w < 6.33$ and 14 well-distributed broad-band stations. For the common calibration events, as well as an additional 247 events ($\sim 1.7 < M_w < \sim 5.0$) not used in either calibration, we find excellent agreement between GIT-derived and CCT-derived source spectra. This confirms the ability of the coda approach to obtain stable source parameters even with few calibration events and stations. Even reducing the coda calibration data set by 75 per cent, we found no appreciable degradation in performance. This validation of the coda calibration approach over a broad range of event size demonstrates that this procedure, once extended to other regions, represents a powerful tool for future routine applications to homogeneously evaluate robust source parameters on a national scale. Furthermore, the coda calibration procedure can homogenize the M_w estimates for small and large events without the necessity of introducing any conversion scale between narrow-band measures such as local magnitude (M_L) and M_w, which has been shown to introduce significant bias.

Key words: Coda waves; Earthquake ground motions; Earthquake source observations; Apparent stress; Source parameters.

1 INTRODUCTION

Many approaches have been proposed throughout the years to estimate source parameters (e.g. seismic moment, corner frequency, radiated energy and apparent stress), such as borehole measurements to avoid near-surface attenuation (Abercrombie 1995; Prejean & Ellsworth 2001), empirical Green's function analysis based on direct waves to remove path and site effects (Ide *et al.* 2003; Prieto *et al.* 2004; Abercrombie 2015) or coda waves (Mayeda & Walter 1996; Mayeda *et al.* 2003, 2007; Walter *et al.* 2017) and data-driven spectral amplitude decomposition approaches (e.g. Andrews 1986; Castro *et al.* 1990; Boatwright *et al.* 1991; Edwards *et al.* 2008; Malagnini *et al.* 2011; Oth *et al.* 2011; Picozzi *et al.* 2017; Trugman & Shearer 2017). Despite so many different novel approaches, it is rare that results from different methods focusing on the same data set yield similar results, and as such, the question of absolute stress drop and its scaling remains quite ambiguous, especially over a broad range of magnitudes (Shearer *et al.* 2019; Kemna *et al.* 2021).

In recent years, methods based on coda envelope measurements have been widely applied in different, complicated tectonic regions (e.g. Eken *et al.* 2004; Morasca *et al.* 2005a, b; Yoo & Mayeda 2013; Gök *et al.* 2016; Holt *et al.* 2021; Shelly *et al.* 2021) demonstrating the ability to obtain stable source measurements over a large frequency range thanks to the stable properties of coda waves (e.g. Aki 1969; Aki & Chouet 1975; Mayeda & Malagnini 2010). The low sensitivity to source and path heterogeneity of coda waves, in fact, allows the assumption of simple 1-D models to adequately describe a region using local to regional events recorded from as few as one station (Mayeda *et al.* 2003). This implies that a limited number of well-recorded events provide stable amplitude measurements over a broad range in magnitudes, for different stations, distances and azimuths when coda waves are used for the analysis.

In this study, we apply the coda calibration technique developed by Mayeda *et al.* (2003) to a calibration data set in Central Italy, composed of 39 events ($3.5 < M_w < 6.33$) and 14 stations. We use a recently developed Java-based code [coda calibration tool (CCT), https://github.com/LLNL/coda-calibration-tool] to obtain a regional calibration useful to derive stable source spectra within the region for future earthquakes. The robustness of the calibration is tested and its performance is evaluated. We find that our results are consistent with prior successful applications of CCT for stable M_w estimation for events too small for reliable waveform modelling and obviate the need for magnitude conversions. These include small local and near-regional events in Utah, Kansas and Oklahoma, eastern Canada and Puerto Rico, respectively, by Holt *et al.* (2021), Shelly *et al.* (2021), Bent *et al.* (2022) and Roman-Nieves *et al.* (2021).

To analyse the performance of the approach in this region, another well-known calibration technique is applied, the generalized inversion technique (GIT; Andrews 1986; Castro *et al.* 1990). The GIT is a heavily data-driven methodology, and given the large amount of high-quality data in Central Italy, it is appropriate for a robust calibration and provides equally stable source parameters in this region. Both CCT and GIT calibrations are then applied to an independent regional data set of 247 earthquakes and the derived source parameters are compared for the validation.

Once the performance of the coda method has been verified in Central Italy, we can apply it to other regions, thereby extending the calibration to a national scale. In fact, taking advantage of the small number of events and stations required for a robust calibration, poorly sampled regions could provide stable measurements as well. This is an opportunity for many future applications of the coda calibration using CCT:

(i) Routine processing for stable estimation of source parameters in quasi-real time.

(ii) Consistent estimation of M_w for small and large events to create a homogeneous seismic catalogue without the necessity of the application of magnitude conversion relationships for small events (e.g. Holt *et al.* 2021; Shelly *et al.* 2021).

(iii) Analysing the behaviour of source scaling relationships in different tectonic environments using a consistent procedure.

The last item focusing on source scaling is especially timely. Following the 2017 Ridgecrest, CA M_w 7.1 main shock and vigorous aftershock sequence, a multi-institutional collaboration was started with the express purpose of understanding the myriad source method's pros and cons. The SCEC/USGS Community Stress Drop Validation Study outlined by Baltay *et al.* (2022) has brought together research groups with very different methodologies with regular discussions that will culminate in a workshop in Fall 2022.

2 DATA SET AND PRE-PROCESSING

For a region with active seismicity and large events, the coda calibration procedure requires a careful selection of good quality data spanning a large magnitude range and distributed spatially. For this study, a set of 39 events ranging between $3.5 < M_w < 6.33$ [values provided by R.B. Herrmann through the St Louis University (SLU) web page, http://eqinfo.eas.slu.edu/eqc/eqc_mt/MECH.IT/] and recorded by 14 well-distributed stations represents the calibration data set (dark blue circles in Fig. 1a) including the main shocks of L'Aquila and Amatrice–Norcia–Visso sequences.

The 14 considered stations are listed in Table 1. Stations FEMA (Monte Fema) and MDAR (Monte Daria) are equipped with an accelerometer, whereas either a velocimeter or both a velocimeter and an accelerometer are operating at all the other stations. We consider only the high sampling rate channels (i.e. 100 and 200 sps for velocimeters and accelerometers, respectively). In terms of site classification, most of the stations are installed in class A (i.e. $vs30 > 800\ m\,s^{-1}$, where vs30 is the average shear wave velocity in the top 30 m) or B ($360\ m\,s^{-1} < vs30 < 800\ m\,s^{-1}$) of Eurocode 8 (CEN 2004); stations FRON, PP3 and SRES are installed on fluvial unconsolidated sediments with $vs30 < 180\ m\,s^{-1}$ (class D).

All data are instrumentally corrected and converted to velocity in $m\,s^{-1}$. The instrument correction procedure dynamically sets the best pre-deconvolution filter parameters on the basis of signal-to-noise analysis. In particular, the high-pass corner frequency of the Butterworth pre-deconvolution filter is the lowest frequency f_{HP} in the range 0.03–2.0 Hz, for which the signal-to-noise ratio (SNR) is always greater than 3 for frequencies between f_{HP} and 2 Hz. The low-pass corner frequency is fixed to 48 Hz, always lower than the Nyquist frequency for the recordings used in this study.

The small number of events and stations needed for this calibration procedure is one of the advantages of analysing coda waves because they are composed of scattered waves averaging the variation of path heterogeneity, source-radiation pattern and directivity (Aki 1969; Aki & Chouet 1975; Mayeda & Malagnini 2010). This implies that the performance of a single-station coda amplitude measurement is comparable to a network average using direct waves (Mayeda & Walter 1996; Mayeda *et al.* 2003).

Although the method requires a small amount of data, for a stable and robust calibration it is important to select high quality

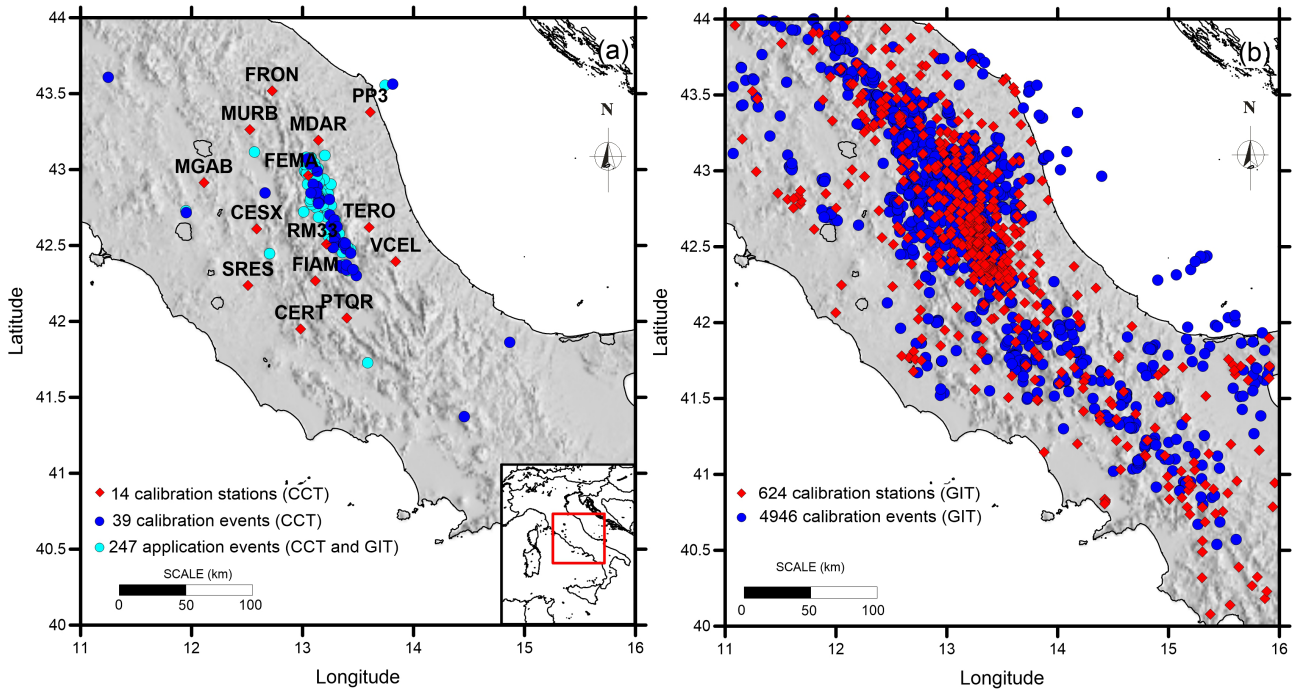

Figure 1. Maps showing the event and station distributions. (a) Data set for coda calibration composed of 39 events (blue circles) and 14 stations (red diamonds). The light blue circles are the 247 events used for the application of both coda- and GIT-derived source parameters. (b) Data set for the GIT calibration based on 4946 events (blue circles) and 624 stations (red diamonds).

Table 1. Stations used for the coda calibration. The last column indicates the site classification based on EC8 as provided by CRISP () database (http://crisp.ingv.it/).

Station	Latitude	Longitude	Channel	Sampling rate (sps)	EC8
CERT	41.94903	12.98176	HH	100	A
CESX	42.60849	12.58676	HH	100	A
FEMA	42.96210	13.04976	HN	200	B
FIAM	42.26802	13.11718	HN and HH	100 (both)	A
FRON	43.51777	12.72572	EH	100	D
MDAR	43.19270	13.14270	HN	200	B
MGAB	42.91263	12.11214	HN and HH	100 (both)	A
MURB	43.26300	12.52460	HN and HH	100 (vel), 200 (acc)	B
PTQR	42.02193	13.40057	HH	100	B
RM33	42.50898	13.21452	HN and EH	100 (both)	B
SRES	42.23696	12.50993	HH	100	D
TERO	42.62000	13.60000	HN and HH	100 (both)	A
VCEL	42.39455	13.84059	EH	100	A
PP3	43.37783	13.60950	HN and EH	100 (vel), 200 (acc)	D

recordings from moderate to large events at both local and regional distances. While the recent seismicity of Central Italy is mainly localized in the region of the 2009 and 2016/2017 sequences (L'Aquila and Amatrice–Norcia–Visso, respectively), to better constrain the path calibrations we also included a few more distant, high-quality moderate events as shown in Fig. 1(a).

A first quality check was manually performed for all event recordings by removing any spurious or bad records, checking for waveform saturation and/or distortion and possible near-field effects.

For each event and station, the two horizontal components are used to form 17 narrow-band envelopes in a range 0.03–25 Hz via Hilbert transform technique and, subsequently log-averaged and smoothed for additional stability. A long window of 1600 s, including 400 s of pre-event, is set to include long-period coda waves for the largest events of the data set.

We point out that coda envelopes are formed for all frequency bands in the considered range, but the corresponding amplitude measurements are used only after a second quality check to ensure a minimum SNR threshold and a critical window length (see Section 3).

A holdout or 'validation' data set of 247 small events (light blue circles in Fig. 1a) is assembled and used to verify the applicability of the estimated calibration parameters for the region. This 'application data set' represents the first step towards future routine applications. The range of magnitude for this data set is roughly 1.7–5.0. All events are recorded by at least 5 of the 14 stations used for the calibration.

Reliable decomposition of *S*-wave spectra into source, propagation and site terms require data sets with a high level of redundancy, that is to say, earthquakes in the data set should be recorded

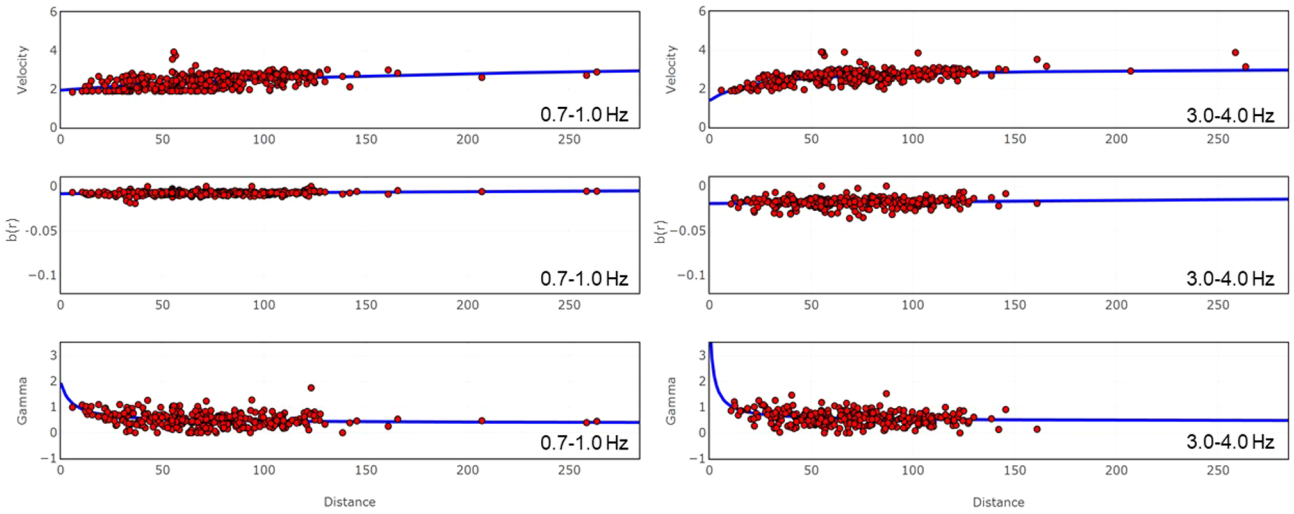

Figure 2. Calibration examples of velocity and envelope shape parameters for two frequency bands (0.7–1.0 Hz and 3.0–4.0 Hz). Solid circles (red) are single envelope measurements and solid lines (blue) are the best-fitting averaged model curves.

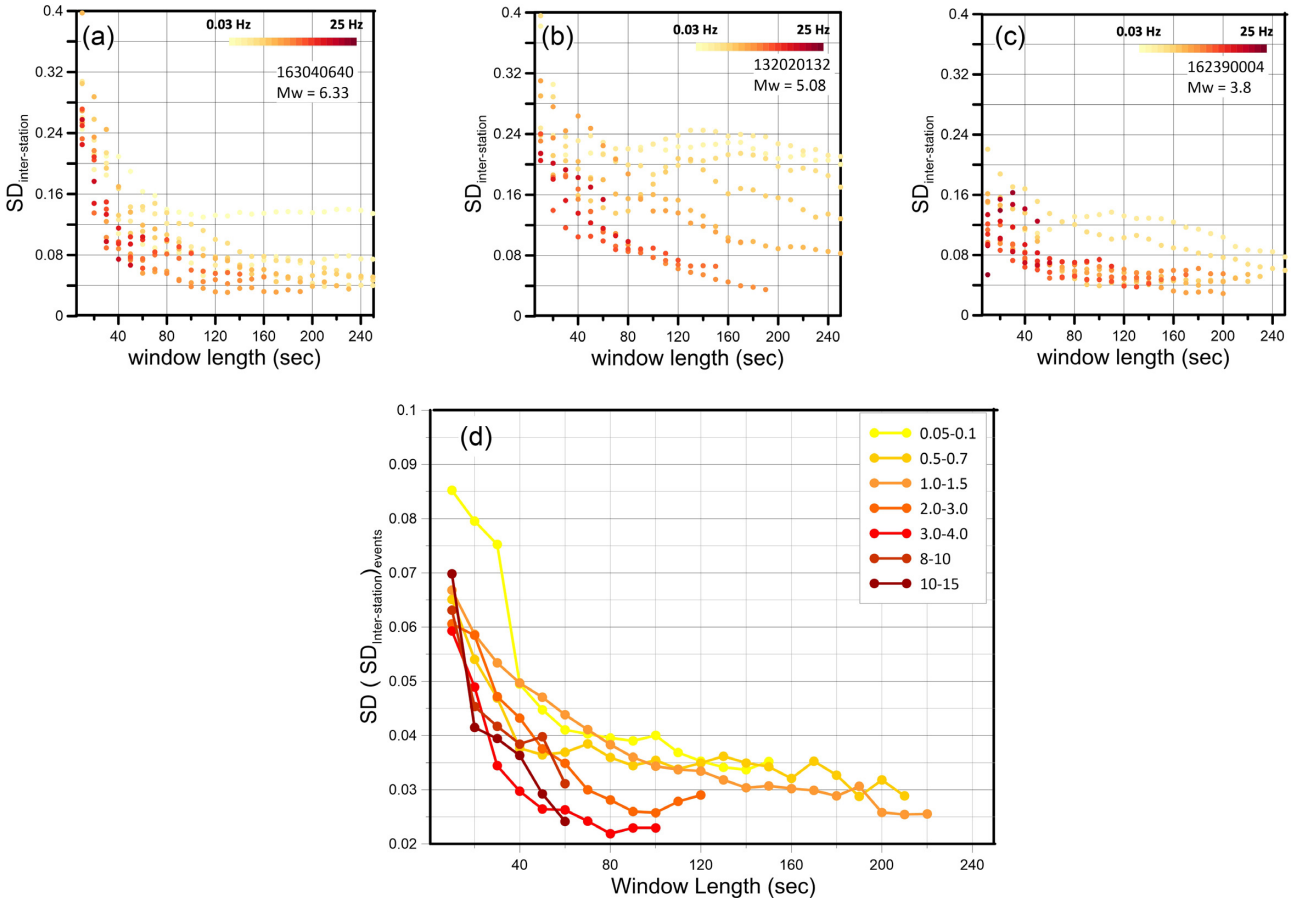

Figure 3. (a–c) Interstation standard deviation versus measurement window length as a function of frequency for three events of different M_w. (d) This figure shows the average interstation standard deviation over all events as a function of the window length for different frequencies and guides our choice of minimum measurement window length.

by a dense seismic network where each station recorded several earthquakes at different azimuths and distances (Bindi *et al.* 2020; Hussein *et al.* 2022). Therefore, GIT was applied to a data set composed of 4946 events recorded by 624 stations (Fig. 1b). In the GIT processing the 247 application events shown in Fig. 1(a) were deliberately excluded.. Fourier amplitude spectra are computed using windows extracted from the horizontal components including *S* waves. Windows are selected starting 0.1 s before the *S* wave onset and ending when distance-dependent percentages of the cumulated squared velocity are reached: 90 per cent for distances $R \leq 25$ km,

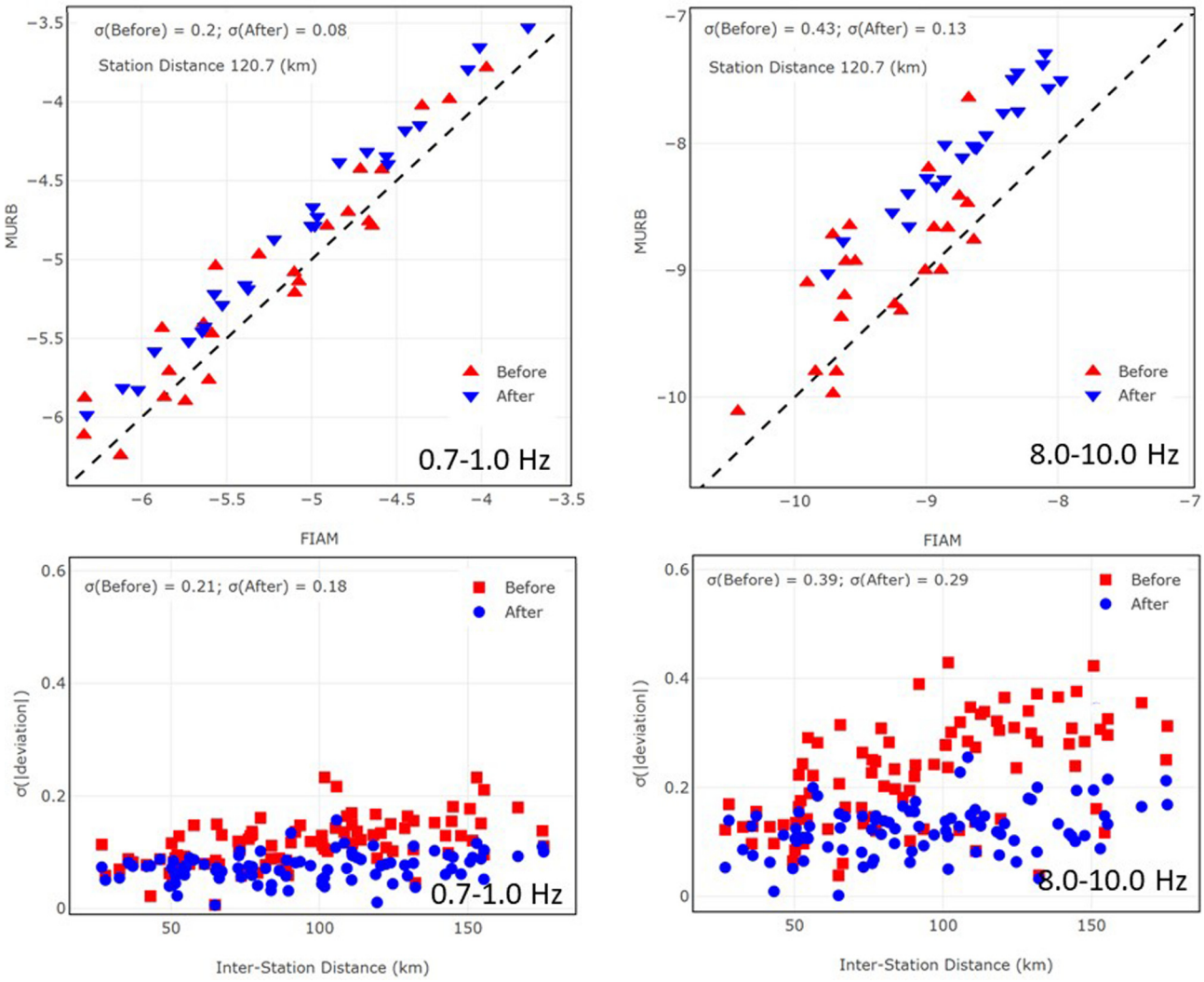

Figure 4. Examples of path correction at 0.7–1.0 Hz (left-hand panel) and 8.0–10.0 Hz (right-hand panel). Top figures show amplitude measurements for common events between stations MURB and FIAM before (red symbols) and after (blue symbols) the application of path correction. Note that for the 8.0–10.0-Hz corrected amplitudes are aligned off the 1:1 line, this is due to the relative site effect between the two stations at the shown frequency bands. Bottom figures show the improvement of standard deviation due to the path correction as a function of interdistance between all pairs of stations.

80 per cent for 25 km $< R \leq$ 50 km; 70 per cent for $R >$ 50 km (Pacor *et al.* 2016a), requiring a minimum duration of 4 s. Spectra are smoothed with Konno & Ohmachi (1998) algorithm, setting the smoothing parameter to 40. The SNR is computed with respect to the pre-event noise window and we set the threshold to 5. Finally, the two horizontal components are summed vectorially.

3 CODA CALIBRATION METHODOLOGY

The coda calibration methodology was developed by Mayeda & Walter (1996) and updated by Mayeda *et al.* (2003) to calibrate regional site and path propagation to correct coda-envelope measurements with the goal of obtaining stable source spectra over a broad range in magnitudes at local and regional distances.

A platform-independent Java-based code was recently developed (CCT, Barno 2017) to simplify and speed up the calibration process outlined by Mayeda *et al.* (2003), thereby significantly reducing the calibration effort required by the user. The CCT, is freely available on GitHub (https://github.com/LLNL/coda-calibration-tool).

Below we describe the main concepts and steps for the calibration procedure applied to the Central Italy calibration data set and refer the reader to Mayeda *et al.* (2003) for more calibration details.

Coda envelopes are formed, as described in the previous section, for 17 different frequency bands in the range 0.03–25 Hz and represent the input to the calibration process.

The coda envelope can be described by the following equation, based in large part on the single-scattering model of Aki (1969), but modified to account for the local and regional distance dependence of all parameters in a single calibration:

$$A_C(f,t,r) = W_0(f).S(f).T(f).P(r,f).H(t-t_S). \\ (t-t_S)^{-\gamma(f,r)} \exp[-b(f,r).(t--t_S)], \quad (1)$$

where $t_S = r/v(f, r)$, f is the centre frequency of the considered band (Hz), t is the time from the origin time (seconds) and r is the epicentral distance (km). $W_0(f)$, $S(f)$ and $T(f)$ represent the S-wave

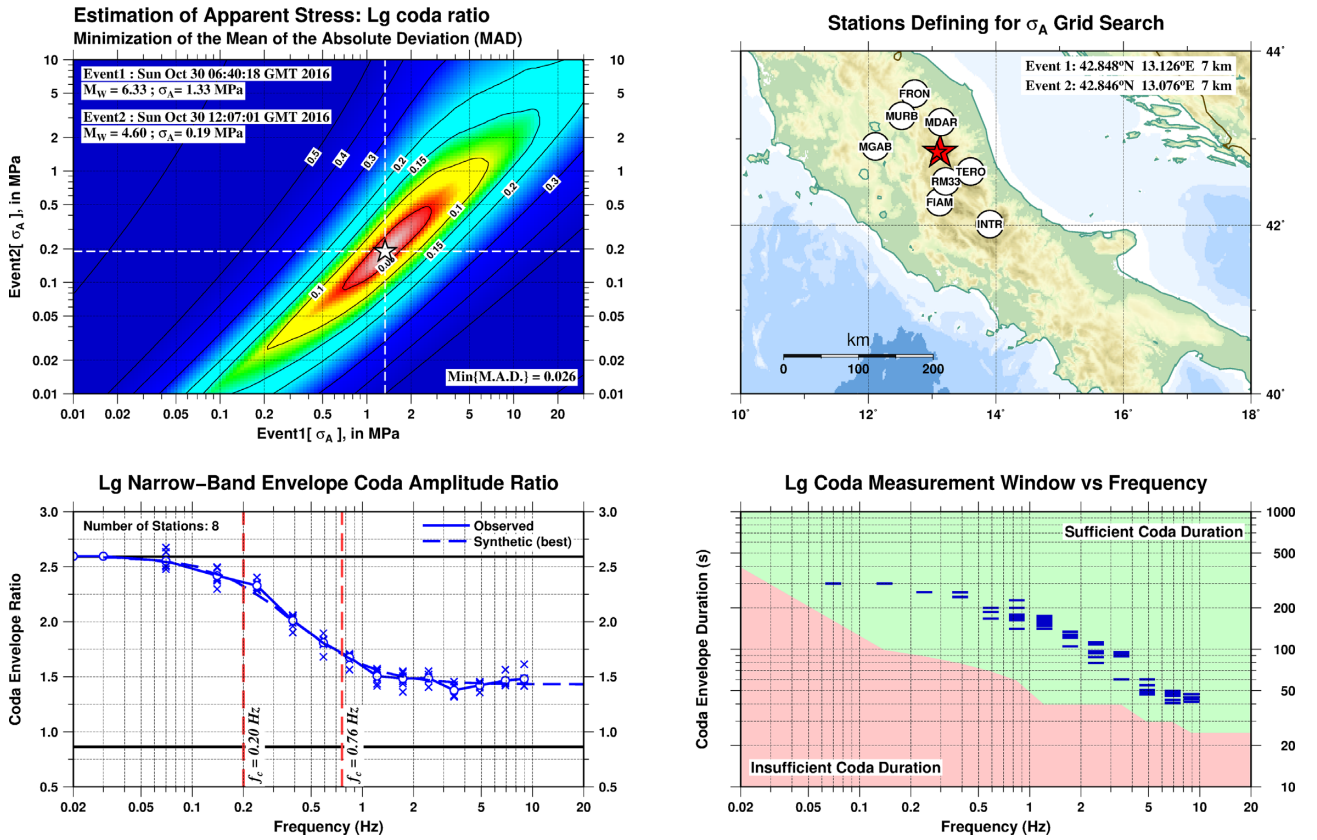

Figure 5. Upper left-hand panel shows example of best apparent stress estimates by minimizing the mean absolute deviation (MAD) from coda spectral ratios taken between the Norcia main shock (30 October 2016 06:40 UTC, M_w 6.33) and an M_w 4.0 aftershock, roughly 5 km away at the same depth. The best-fitting theoretical Brune (1970) source spectra (blue line) are used as reference GT events for site calibration (lower left-hand panel). For the eight stations that we used, the ratios show no variability with distance or azimuth and all have sufficiently long coda envelopes based on the empirical minimum window length results of Mayeda *et al.* (2003) and in Fig. 3 (lower right).

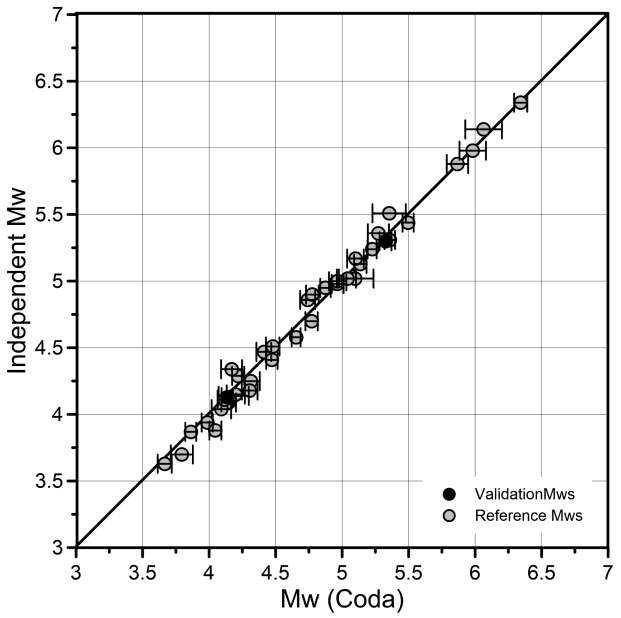

Figure 6. Reference (grey circles) and validation (black circles) moment magnitudes compared to the coda-derived M_w's obtained from the calibration analysis in Central Italy. The independent M_w's are available from regional moment tensor analysis (R.B. Herrmann through the SLU web page, http://eqinfo.eas.slu.edu/eqc/eqc_mt/MECH.IT/). The 1:1 line is also shown as a reference.

source, site effect and *S*-to-coda transfer function, respectively. The anelastic attenuation and the geometrical spreading are described by $P(r, f)$, H is the Heaviside step function, $v(f, r)$ is the peak velocity (in km s^{-1}) and $b(f,r)$ and $\gamma(f,r)$ are parameters controlling the coda envelope shape.

As each region often has a unique coda-envelope decay (e.g. Sato & Fehler 1998), the first step of the calibration process requires the definition of envelope shape parameters ([$b(f,r)$ and $\gamma(f,r)$)] to form synthetic envelopes to be used to measure coda amplitudes through a match with observed envelopes (see Mayeda *et al.* 2003, for more details). Furthermore, for each envelope the time corresponding to the peak velocity is a necessary piece of information to define the coda measurement start point as it corresponds to the direct-*S* or surface wave arrival time. It is done in terms of a regionally calibrated velocity parameter, $v(f, r)$. These three parameters are empirically calibrated for each frequency using simple hyperbolic distance-dependent functions. Fig. 2 shows an example for two frequency bands where average models are determined to describe these parameters as a function of distance. In simple terms, this *ad hoc* parametrization allows us to combine, in a single calibration, envelopes derived from *S* waves, regional L_g waves, and surface waves at a range of distances, spanning local to regional distances.

The synthetic envelopes are generated for each frequency and distance using eq. (1) by ignoring at first, source, path, site and transfer function effects (set to unity) because the coda envelope shape is controlled only by the time-dependent terms of the equation (Mayeda *et al.* 2003).

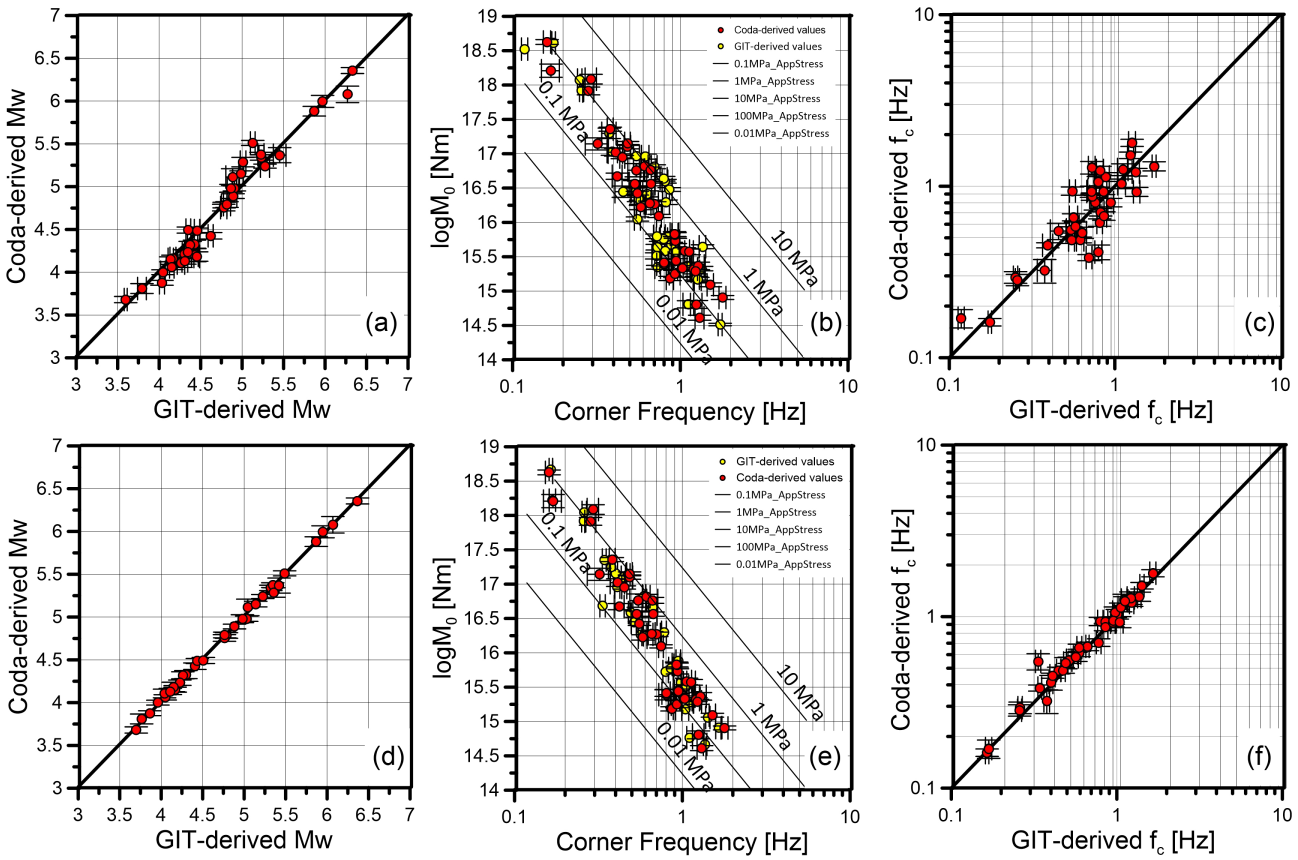

Figure 7. Coda-derived versus GIT-derived source parameters for the common calibration events. (a) Comparison of M_w values shown with the 1:1 line for reference; (b) seismic moment versus corner frequency relationship from coda (red) and GIT (yellow) analysis with lines of constant apparent stress for reference; (c) corner frequency estimates shown with the 1:1 line for reference. Figs 7(d)–(f) show the results obtained by constraining the seismic moment of individual events to the values provided by CCT and fitting only for f_c. The comparison in Fig. 7(f) shows that in this case the corner frequencies are in excellent agreement, with only one outlier event (132 020 132) deviating from the one-to-one line.

Then for each event and station, coda amplitudes are measured for consecutive frequencies as a constant or DC shift of the synthetic curve generated at the appropriate distance to fit the observed envelope using an L-1 norm. These raw amplitudes are initially non-dimensional as path and site effects have yet to be removed.

Although a pre-selection is performed on the recordings as explained in Section 2, coda amplitudes are subject to further selection criteria to avoid calibrating the parameters using poor quality envelopes. This means that for some envelopes the amplitude measurement is discarded on the basis of frequency-dependent criteria based on a minimum SNR threshold and a critical window length. In fact the stability of the measured amplitudes can be affected by the window-length choice (Mayeda *et al.* 2003) that is also correlated to the SNR.

For the calibration events, the window length is manually selected on each envelope considering a frequency-dependent SNR threshold. Figs 3(a)–(c) show some examples of variation of interstation standard deviation as a function of measurement window length for three events. A short measurement window length results in a large scatter for amplitude measurements at different stations for the same frequency band. Increasing the measurement window length we observe a rapid decrease in the interstation standard deviation, stabilizing at a minimum representing the critical time length beyond which the interstation scatter stabilizes. Analysing all events for different window lengths (Fig. 3d), we identified the optimal window lengths for each band.

Path corrections are empirically based and meant to mimic observed local and near regional coda observations. Unlike direct waves which decay immediately with distance due to geometrical spreading and attenuation, coda at local distances at the same time relative to the origin time are roughly homogeneous (Aki 1969; fig. 8 of Mayeda *et al.* 1992) and then decreases slowly with increasing distance. The basic idea is to find the parameters that minimize interstation scatter for common events between pairs of stations, as shown in the example of Fig. 4(top panels) for the frequency bands 0.7–1.0 Hz and 8.0–10.0 Hz. Considering multiple station combinations, it is possible to verify the stability of the corrections over a wide distance range (Fig. 4, bottom panels). The figure shows that for Central Italy path-corrected coda amplitudes (blue symbols) are distance independent at least up to 200 km, as the interstation scatter remains almost constant for all pairs of stations. This is an indication of the efficacy of the empirically derived 1-D path correction, and was evaluated for all frequency bands in the analysed range.

The final step of the calibration is to correct the coda amplitudes for *S*-to-coda transfer function and the relative site effects, transforming the dimensionless, distance-corrected amplitudes into moment-rate spectra in units of N-m. This final step requires independent estimates of source parameters for some events in the data set to be used as references (Mayeda *et al.* 2003).

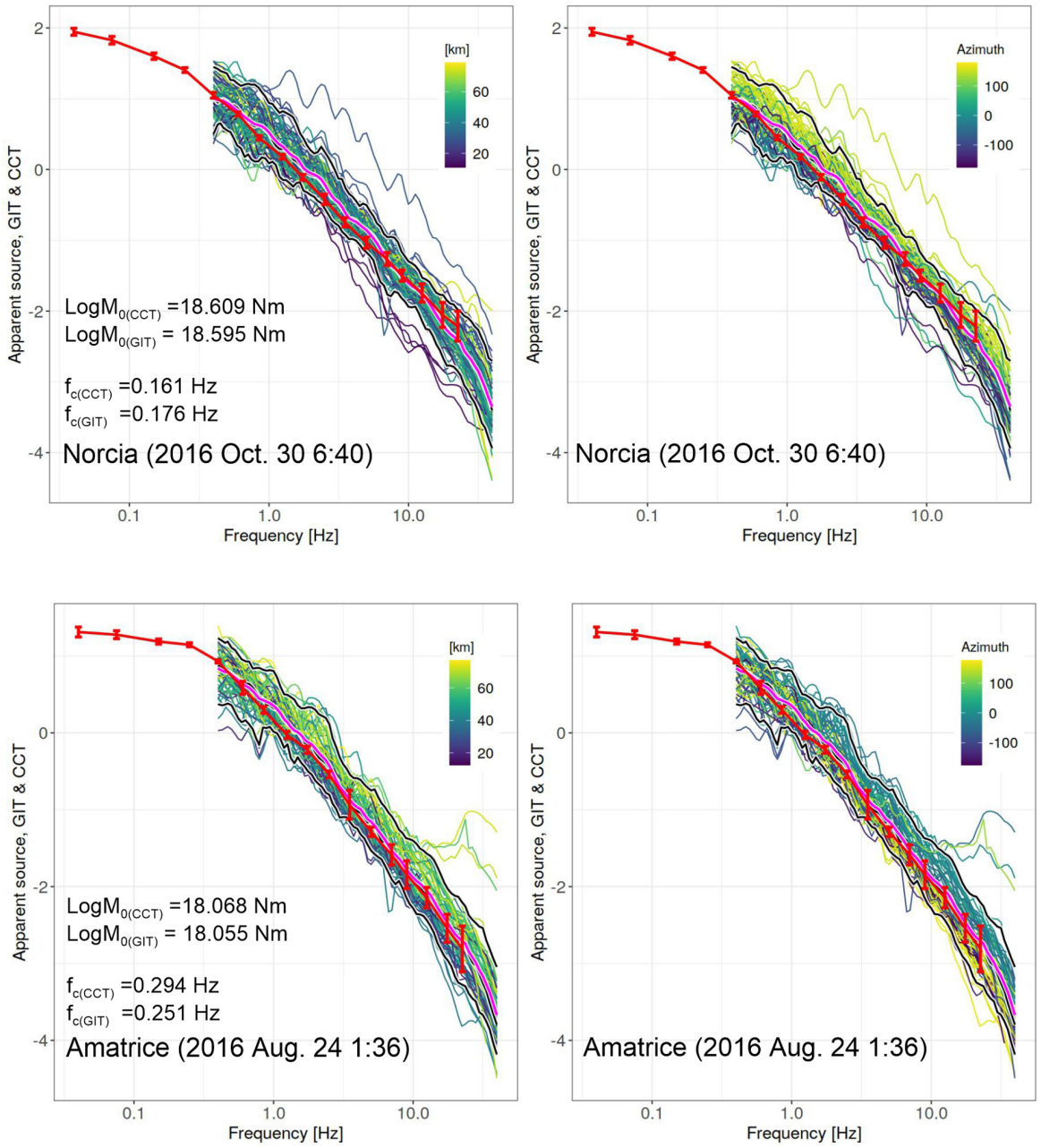

Figure 8. Spectral shape comparison for two calibration events (Norcia, 2016 October 30, 6:40 UTC M_w 6.33 and Amatrice, 2016 August 24, 01:36 UTC M_w 5.97). In general, the averaged coda-derived source spectra (red in these figures) are calculated over a frequency range of 0.03–25 Hz (where possible). Thick magenta lines represent the median GIT spectra for the same two events. The 5th and 95th percentiles are shown as thin black lines in all figures. Coloured curves represent apparent sources as a function of distance (left-hand panel) and azimuth (right-hand panel).

3.1 Reference events and determination of apparent stress for ground-truth (GT)

The original coda calibration procedure (Mayeda & Walter 1996; Mayeda *et al.* 2003) used independent M_w's (e.g. long-period moments) to constrain the frequency dependent site and *S*-to-coda transfer function terms at low frequency and tie the dimensionless, distance-corrected amplitude to an absolute scale (i.e. convert to units in N-m). In other words, the site and transfer function correction at each frequency is the numerical difference between the known moment value and the dimensionless amplitude, and by using multiple reference events, we can obtain stable, averaged correction terms.

The use of independent M_w's spanning over a broad range allows for reasonable estimates of site corrections up to ~2 Hz for an (M_w ~3.5, Mayeda *et al.* 2003). However, to define site corrections for events at higher frequencies above 2 Hz, small events were used as EGFs (empirical Green's functions) assuming a flat source spectrum for a wide frequency range.

More recently however, and also in this current study, we apply a different approach to better constrain the high frequency site terms based on ground truth (GT) reference spectra, for which apparent stresses are independently calculated through the coda spectral ratio method outlined by Mayeda *et al.* (2007) and applied to numerous global crustal data sets (Malagnini *et al.* 2014).

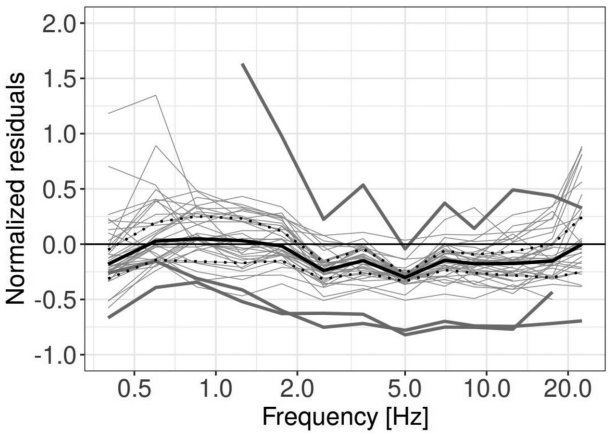

Figure 9. Normalized residuals for calibration events showing the good correspondence between source spectra produced by CCT and GIT techniques. Normalized residuals are computed as the difference between CCT and GIT spectral values normalized to the GIT spectral value. The black line represents the median value of the residual for each frequency and the dotted lines measure the dispersion as median ± MAD (median absolute deviation). Grey lines show the results for each event; thick grey lines indicate the results for three events showing significant discrepancy between the GIT and CCT results, as shown in Fig. S3.

Using independent apparent stress and M_0 for a few reference events, for each station we are able to derive the corresponding site and transfer function terms for the whole frequency range without having to assume any regional source scaling or imposing a stress drop for selected small events as Green's functions that can introduce bias (e.g. Baltay *et al.* 2010, 2011).

The coda spectral ratio method provides very stable, averaged apparent stress estimates that are free of path, site, and source mechanism effects. Fig. 5 shows an example of apparent stress calculation using coda spectral ratios taken between the Norcia main shock (Oct 30, 2016 06:40 UTC, M_w 6.33) and an M_w 4.0 aftershock roughly 5 km away measured by eight surrounding stations. The best-fitting corner frequencies assuming the Brune (1970, 1971) omega-square source model are estimated by minimizing the mean absolute deviation (MAD) between the observed and the synthetic coda spectral ratio. As during the coda calibration, a minimum coda duration is required prior to incorporating the station observation in the network average. Because the stations and paths are common, and the coda averages over the mechanism effects, we obtain very stable source ratios. Next, we use the resulting GT source spectra (apparent stress of 1.33 and 0.19 MPa, respectively) as source constraints to determine all site correction terms for the entire network of stations. Again, this eliminates the need for an assumed source scaling for the region which could otherwise bias the amplitudes at higher frequencies.

In summary, we used independent moment magnitudes from regional moment tensor analysis provided by R.B. Herrmann through the St Louis University (SLU) web page (http://eqinfo.eas.slu.edu/eqc/eqc_mt/MECH.IT/), where 37 were used as reference and the others as validation (Fig. 6). Combined with 4 GT source spectra, these were used as reference source input into the CCT JSON (JavaScript Object Notation) calibration file (Table S1).

4 SPECTRAL AMPLITUDE DECOMPOSITION

The spectral amplitude decomposition approach applied in this study is often referred to as GIT (e.g. Andrews 1986; Castro *et al.* 1990). GIT relies on the assumption that the Fourier amplitude spectrum of the selected *S*-wave (or *P*-wave) windows can be expressed, after removing the instrumental response, as the product of three terms representing the source (S), propagation (A) and site (Z) contributions to ground motion:

$$\log \mathrm{FAS}_{ij}\left(R_{ij}, f\right) = \log S_i\left(f\right) + \log A\left(R_{ij}, f\right) + \log Z_j\left(f\right), \tag{2}$$

where the Fourier amplitude spectrum FAS_{ij} is computed for each selected earthquake i recorded at stations j located at hypocentral distance R_{ij}. In eq. (2), f is the frequency and, in the remainder of this study, we use log to indicate the logarithm with base 10. When the data set is characterized by a large degree of redundancy, that is, the same event is recorded by many stations located at different distances and each station recorded several earthquakes, the overdetermined system (eq. 2) can be solved following a non-parametric approach (Castro *et al.* 1990; Oth *et al.* 2011). To determine the spectral attenuation, we discretize distances up to 80 km into bins 2.5 km wide, and distances between 80 and 150 km into bins 10 km wide. A linear interpolation of the attenuation values is applied between two consecutive nodes and the overall attenuation with distance is smoothed by setting to zero the Laplacian with distance (Castro *et al.* 1990). Since the linear system (eq. 2) is characterized by two unresolved degrees of freedom, two *a priori* constraints have to be added to break the trade-offs between the three terms, producing solutions relative to the assumptions. We introduce a reference distance $R_{\mathrm{ref}} = 5$ km for the attenuation such that $\log A(R_{\mathrm{ref}},f) = 0$ irrespective of the frequency (i.e. the sources are scaled at 5 km), and we assume a reference site condition for the site amplification term Z. Following previous studies performed for the same area (Pacor *et al.* 2016a; Bindi *et al.* 2017), we impose that the average amplification of three selected stations (i.e. Leonessa, LSS; San Martino d'Ocre, RM03 and Spina Nuova, T1221) is equal to the amplification generated by a crustal velocity model with vs30 equal to 760 m s^{-1} multiplied by an exponential term $\exp(-\pi k_0 f)$ (Campbell & Boore 2016). Following Pacor *et al.* (2016a), we use $k_0 = 0.018$ s. We solve the linear system in a least-squares sense (Koenker & Ng 2017) and the results of the spectral amplitude decomposition are shown in Fig. S1. In particular, Fig. S1(a) shows the non-parametric and frequency-dependent attenuation values, whereas Figs S1(b) and (c) show the site amplification terms and the source spectra as isolated by the GIT decomposition, respectively.

Then, the non-parametric source spectra $S(f)$ shown in Fig. S1(c) are fit to a standard omega-square model to estimate the seismic moment M_o and corner frequency f_c

$$\log S(f) = \log K + \log M_o + \frac{1}{1+\left(\frac{f}{f_c}\right)^2}, \tag{3}$$

where the constant K includes all the parameters connecting the low-frequency level of the far-field source displacement to the seismic moment. The constant K is determined by requiring that events in the calibration data set have, on average, the same seismic moment as determined by CCT. To mitigate the effect of the limited bandwidth, the seismic moment of events with magnitude $M_w > 5.5$ are constrained to the values extracted from Herrmann's catalogue. Given the seismic moment and the corner frequency, the stress drop

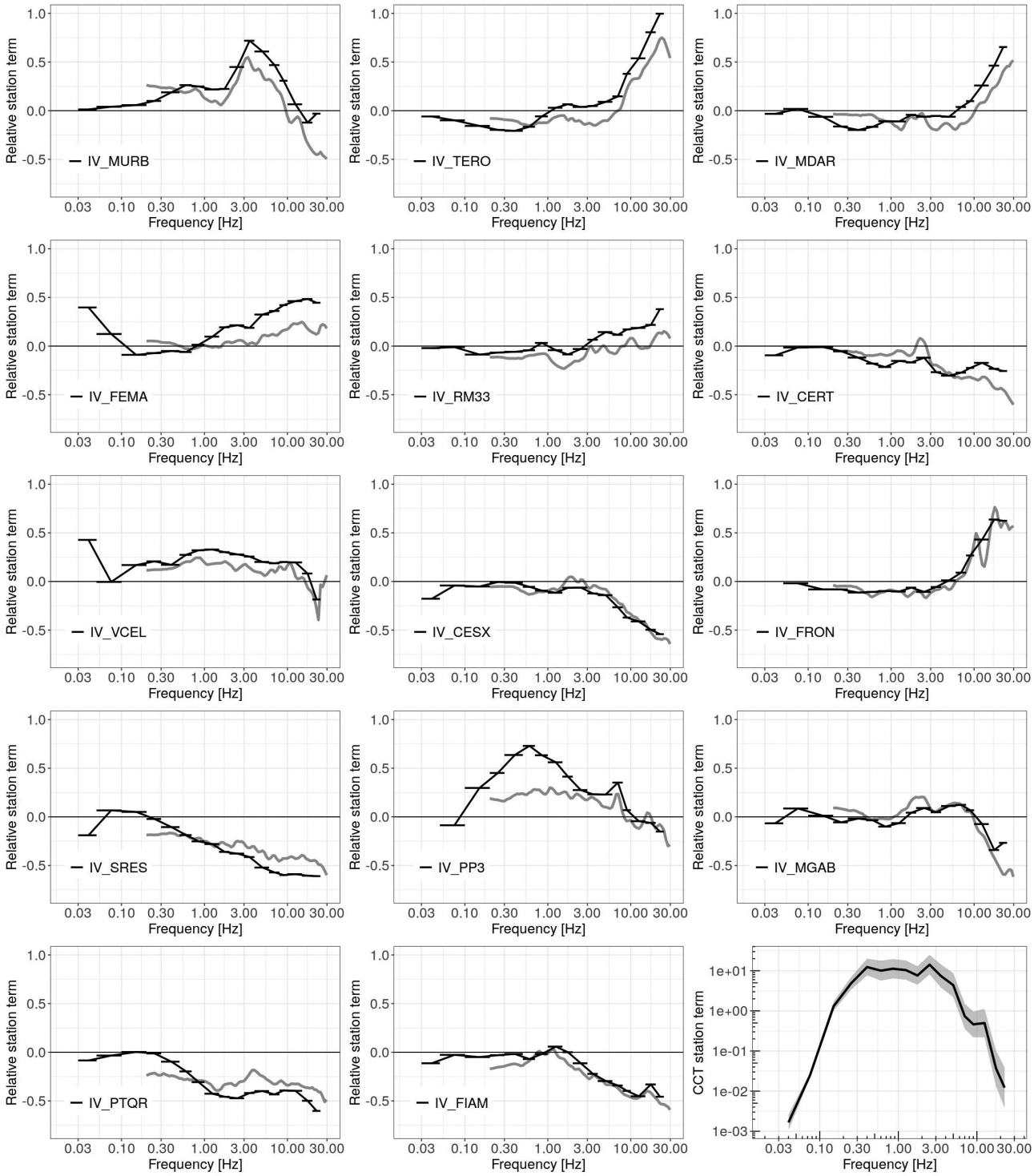

Figure 10. Site terms comparison obtained from CCT (black curves) and GIT (grey curves) for the 14 stations used for the coda calibration. The site terms have been normalized to the mean of the 14 stations. In the bottom right-hand panel, the mean ± 1 standard deviation of the unscaled CCT site terms is shown.

$\Delta\sigma$ is computed from the source radius r using (Eshelby 1957; Keilis-Borok 1959; Madariaga 1976, 1979)

$$\Delta\sigma = \frac{7}{16}\frac{M_o}{r^3}, \tag{4}$$

$$r = \frac{k\beta}{f_c}, \tag{5}$$

where $k = 0.37$ (Brune 1970, 1971) and $\beta = 3.2$ km s^{-1} are used. For an omega-square source model, we note that apparent stress, which is proportional to the ratio of total radiated seismic energy to seismic moment ($\tau_a = \mu E_s/M_o$) is related to the Brune static stress drop (Wyss & Brune 1968) as $\tau_a = \Delta\sigma/4.3$ (Singh & Ordaz 1994). For the events used in the GIT decomposition, Es is computed from the integral of the non-parametric source spectra, mitigating

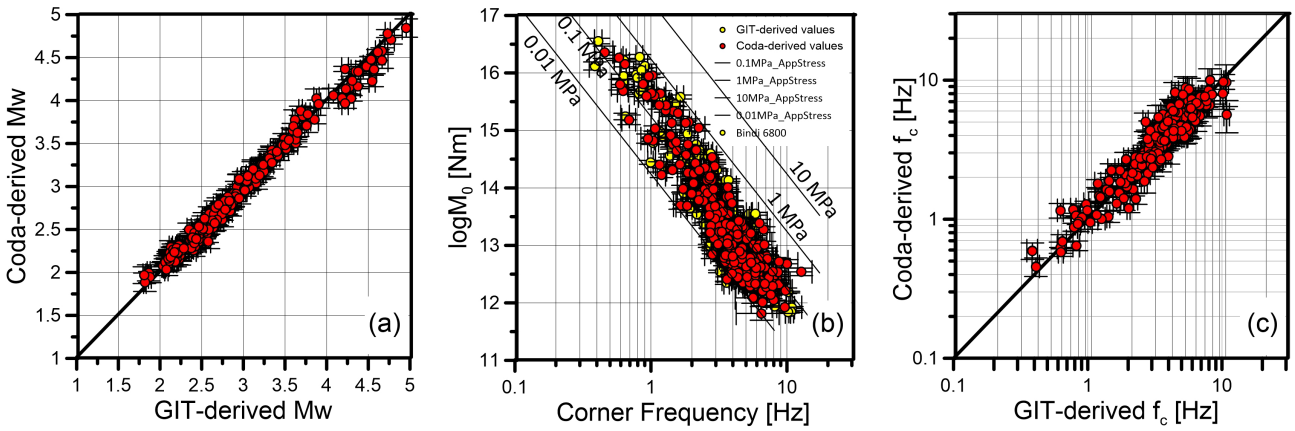

Figure 11. Coda-derived versus GIT-derived source parameters for the 247 application events that were held out of both calibrations. (a) Comparison of M_w values, where the line 1:1 is shown for reference; (b) seismic moment versus corner frequency relationship from coda (red) and GIT (yellow) analysis with lines of constant apparent stress for reference and (C) corner frequency estimates also show excellent correspondence, where the line 1:1 is shown for reference.

finite bandwidth effects by asymptotically extrapolating the source spectra with an omega-square model. The comparison between apparent stress and Brune stress drop is shown in Fig. S2; the best-fitting line has slope 0.2478 = 1/4.03 and is close to the expected theoretical value, confirming the suitability of the model assumed to compute the source parameters.

5 RESULTS

5.1 Calibration comparisons

A first step to analyse the quality of source parameters derived from the coda calibration with respect to those from GIT, is to compare results for the common calibration events included in both calibration processes. Fig. 7 shows source parameters obtained for the 34 identified common events. In general, the parameters are in good agreement, although GIT-derived M_w's are slightly underestimated for the range ∼4.7–5.2 and overestimated for the range ∼4.0–4.5 (Fig. 7a). As observed in Fig. 6 for the same range of magnitude, the coda-derived M_w's do not show any unexpected trend. Therefore, it is possible that the spectral fitting applied to the GIT spectra for magnitude around 5 was affected by limited bandwidth extension toward low frequencies. The corner frequencies estimated from the CCT and GIT spectra are in good agreement (Fig. 7c), as their average difference is equal to 0.03 Hz, with standard deviation 0.24 Hz. Since the GIT source spectra are defined above 0.3 Hz, the lack of low frequencies could result in a trade-off between M_0 and f_c when performing the least-squares fit for calibration events. Conversely, the CCTs spectra are evaluated over much lower frequencies, allowing for more robust seismic moment estimations. Therefore, in order to evaluate the impact of possible limited-bandwidth effects on source parameters estimated from the GIT source spectra, Figs 7(d)–(f) show the results obtained by repeating the fit over the same GIT source spectra as in Figs 7(a)–(c) but constraining the seismic moment of individual events to the values provided by CCT and fitting only for f_c. The comparison in Fig. 7(f) shows that in this case the corner frequencies are in excellent agreement highlighting the high similarity between GIT and CCT source spectra over the common bandwidth, with only one outlier event (132 020 132) deviating from the one-to-one line (the difference between CCT and GIT corner frequencies for this event is equal to 0.21 Hz). The source spectra of event 132 020 132 are shown in Fig. S3.

The comparison in terms of spectral shape demonstrates the similarity of the results over a large frequency range (0.4–25 Hz is the common range covered by both calibration approaches). Fig. 8 shows the Norcia (2016 October 30, 06:40 UTC) and Amatrice (2016 August 24, 01:36 UTC) main shocks as two examples of spectral shape comparison. Coda-derived spectra (red curves, shown over the whole frequency range analysed with this method) are within the 5th and 95th percentile of GIT results in all cases, and in general overlap the median GIT-derived spectra. Colour curves represent the GIT-derived apparent sources as a function of distance and azimuth, demonstrating that for these events the coverage is excellent and spectral estimates are very robust. Most striking is the strong azimuthal dependence for the Norcia main shock *S*-wave spectra from GIT, whereas the corresponding coda-derived spectra sits in the mean of the direct wave spectral population, further verifying the averaging nature of coda.

The overall agreement between the observed GIT and CCT source spectra is summarized in Fig. 9, where the frequency-dependent differences between the CCT and GIT spectral values normalized by the GIT values are shown for the 34 common calibration events. For each frequency, the median normalized difference (black line) ±1 median absolute deviation (dotted lines) are also shown. The source spectra for the three events showing the largest discrepancy are shown in the electronic supplement (Fig. S3) and we briefly describe potential reasons for the discrepancy in the following.

For event 143 531 036, we observed a distinct spectral bump at ∼4 Hz in the direct spectra and unlike any other spectra in the data set. One possibility is that this is a doublet but one would expect to see this in the coda spectra as well. A more likely reason is this event is at the margins of the CCT calibration region and recorded by only three stations for the CCT analysis which may account for it having lower amplitude than the direct wave average.

For event 161 512 024, we observe a distinctive spectral peak in the ∼0.3–0.7 Hz range, which has been observed in other regions for shallow sources (e.g. mine collapse events, shallow explosions, shallow earthquakes) when using the same coda source spectral method (e.g. Mayeda & Walter 1996; Murphy *et al.* 2009). One hypothesis is that this is a very shallow earthquake and the peak is due to strong R_g-to-*S* scattering conversion due to excitation of

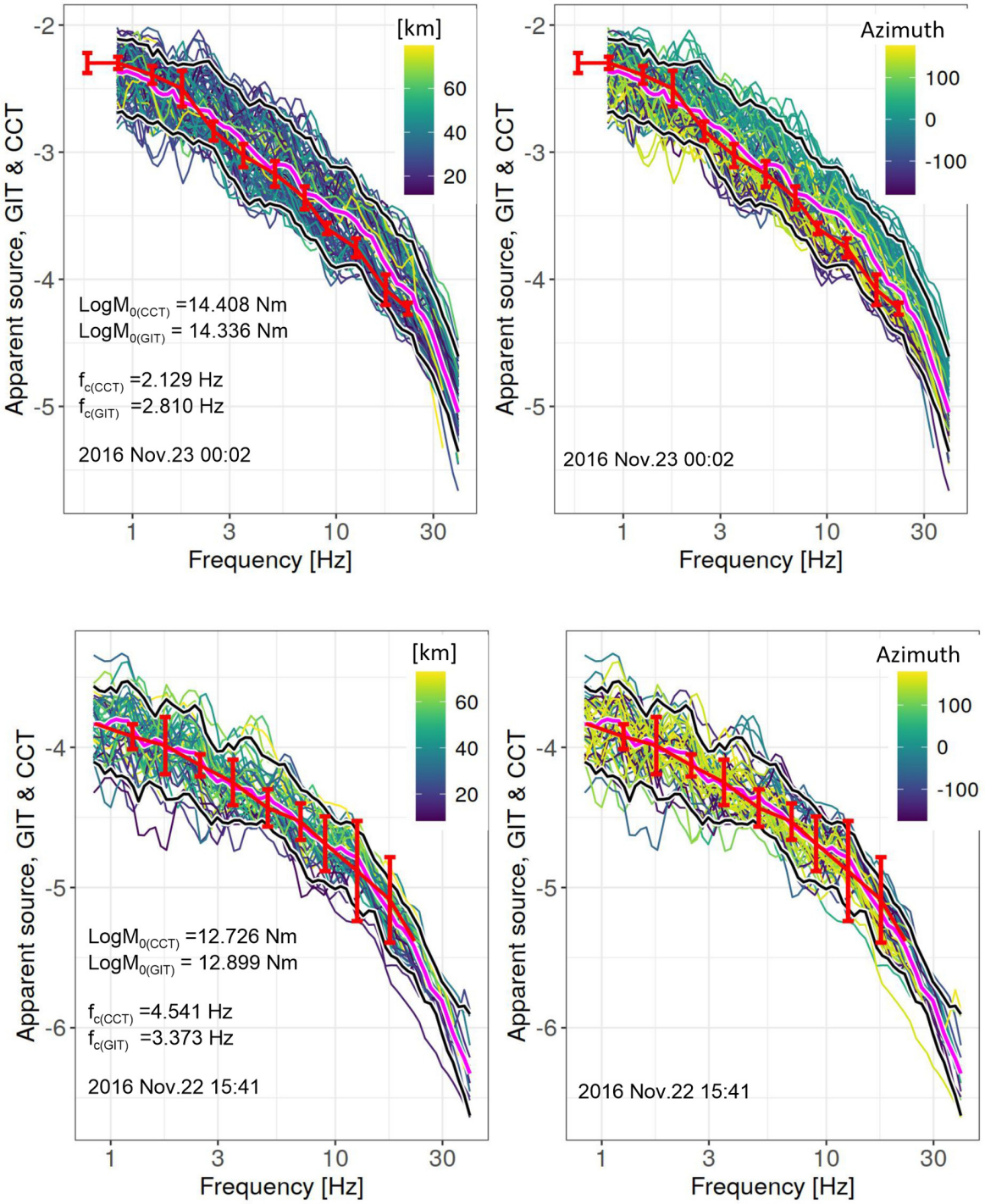

Figure 12. Spectral shape comparison for two events from the application data set (2016 November 23 00:02 UTC M_w 3.52 and 2016 November 22 15:41 UTC M_w 2.40). Coda-derived source spectra (red) are averaged over all stations. Thick magenta lines represent the median GIT spectra for the same two events. The 5th and 95th percentiles are shown as thin black lines in all figures. Coloured curves represent apparent sources as a function of distance (left-hand panel) and azimuth (right-hand panel).

R_g for shallow sources and scattering into the coda due to near surface impedance contrast. Furthermore, shallow event spectral fall-off tends to be steeper than omega-square (Mayeda & Walter 1996; Murphy *et al.* 2009), possibly due to near-surface attenuation that absorbs the high frequency coda, in contrast to direct *S* which may be escaping through the bottom of the focal sphere without too much loss.

Additionally, for event 132 020 132 we observe good agreement at high frequencies but it appears that the GIT low frequency spectral level is too low and subsequently is pushing the corner frequency estimate lower than the coda-derived spectra (see Fig. 7f). This event is characterized by a large azimuthal gap of ∼220° as the event sits offshore and thus one possible explanation is that the GIT source spectra are affected by directivity (Pacor *et al.* 2016b) or focal

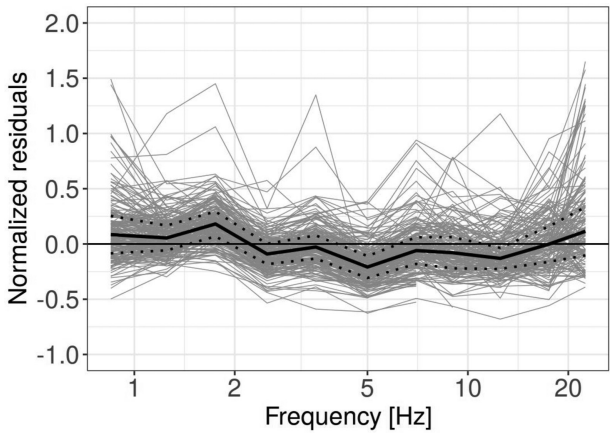

Figure 13. Normalized residuals for application events also show good correspondence between source spectra produced by CCT and GIT techniques. The black line represents the median value of the residual for each frequency and the dotted lines measure the dispersion as median ± MAD (Median Absolute Deviation). Grey lines show the results for each event. Normalized residuals are computed as the difference between CCT and GIT spectral values normalized to the GIT spectral value.

mechanism effects not averaged out by the azimuthal coverage of the stations.

Finally, we compare relative, weak-motion site terms from the two approaches and unsurprisingly (e.g. Aki 1980; Kato *et al.* 1995), find excellent agreement between them for common pass bands, as expected by the dominance of *S* waves in the scattered field (Aki 1992; Zeng 1993). Fig. 10 shows individual site terms relative to the network average results for 14 stations used in the coda calibration along with the average CCT station-site transfer term which all individual stations were compared against. The only striking amplification difference is observed below 2- Hz at station PP3, one of the stations installed on unconsolidated sediments (Table 1). Although several studies investigating the consistency of the *S*-wave and coda-wave site amplifications found a similarity of the results within a factor between 1.5 and 2 (Kato *et al.* 1995; Bonilla *et al.* 1997), a few larger discrepancies were observed either for stations installed over deep sediments (Margheriti *et al.* 1994) or when recordings at epicentral distances smaller than the focal depth were analysed (Su *et al.* 1996). Phillips & Aki (1986) also observed some cases of basin resonance for intermediate period coda in central California, which might explain our amplification at station PP3 relative to direct wave amplification. Further investigations are needed to understand whether complicated resonant waves could be the explanation for the observed differences in CCT and GIT station terms obtained for PP3.

5.2 Small events application and comparison

For a more significant validation we applied both GIT and CCT calibration parameters to the holdout data set composed of 247 events ($\sim 1.7 < M_w < \sim 5.0$) recorded in the same region. The GIT source spectra are computed as the median of the apparent source spectra obtained by correcting the recorded spectra considering the non-parametric attenuation model and site effects isolated by the spectral decomposition.

This comparison has a dual function: First, it validates the results of the coda calibration approach and second, it confirms the CCT can be used in near real-time analysis to create catalogues characterized by homogeneous and reliable estimates of source parameters for small and large events using a common method. For example, Shelly *et al*. (2022) warned that large biases can be introduced when attempting to tie local magnitudes (i.e. M_D, M_L, etc.) to M_w for small events that cannot be waveform modelled.

Fig. 11 demonstrates that both GIT and coda-based calibrations provide source parameters in excellent agreement down to $M_w \sim 1.7$ confirming the good performance of both approaches in this region with the advantage that the coda technique requires a small number of events and stations to obtain the same stability of a data-driven technique as GIT.

The spectral shapes are also consistent between the two approaches (Fig. 12), although with larger variability with respect to the results obtained with the calibration events (Fig. 8). This is not unexpected since we are looking at events not included in the calibration and characterized by smaller magnitudes with potentially fewer recording stations, lower SNR and shorter window lengths. Despite these issues, the average coda-derived spectra remain within the 5th and 95th percentile evaluated by the GIT analysis, with resultant stable estimates of source parameters for all the 247 events. The similarity of the GIT and CCT source spectra for the application data set is confirmed in Fig. 13 where we show that the median normalized residuals are close to zero, free of any frequency-dependent trend, and with a median absolute deviation ranging only between 10 and 20 per cent of the GIT spectral values.

5.3 Robustness test

To test the robustness of the coda calibration procedure, we performed a series of tests repeating the calibration by progressively reducing the number of events and stations by 50 and 75 per cent with respect to the original calibration based on 39 events and 14 stations (best case). The M_w ratio between the best case and the tested calibrations remains close to unity in all cases, including the last one (test #6) where we reduced both station and events by 75 per cent simulating a very sparse network (Fig. 14a). Similarly for the corner frequency ratio (Fig. 14c) we observe substantial consistency for all tests.

To confirm the observed robustness of the estimates provided by the CCT using few events and stations, we apply the calibrated parameters obtained for each test to the application data set of 247 events. Figs 14(b) and (d) show that the reduction of calibration events and stations do not adversely affect the final M_w and f_c estimates calculated for new events in the same region, although the variability increases with respect to the calibration events as already described in the previous section.

6 DISCUSSION AND CONCLUSIONS

In this study, we investigate the performance of a well-known approach, the coda calibration methodology (Mayeda & Walter 1996; Mayeda *et al.* 2003), to estimate source parameters for small-to-moderate earthquakes occurring in Central Italy.

To facilitate coda calibration and processing we use the freely available CCT (https://github.com/LLNL/coda-calibration-tool), a Java-based code that implements the method. The strength of this approach is that it requires a limited, but high-quality data set for the calibration, and for Central Italy we selected 39 events ranging between M_w 3.5 and 6.33 and 14 well-distributed stations. The calibrated coda parameters were then applied to a validation or 'application' data set composed of 247 earthquakes that were excluded from both the CCT and GIT calibration processes. These

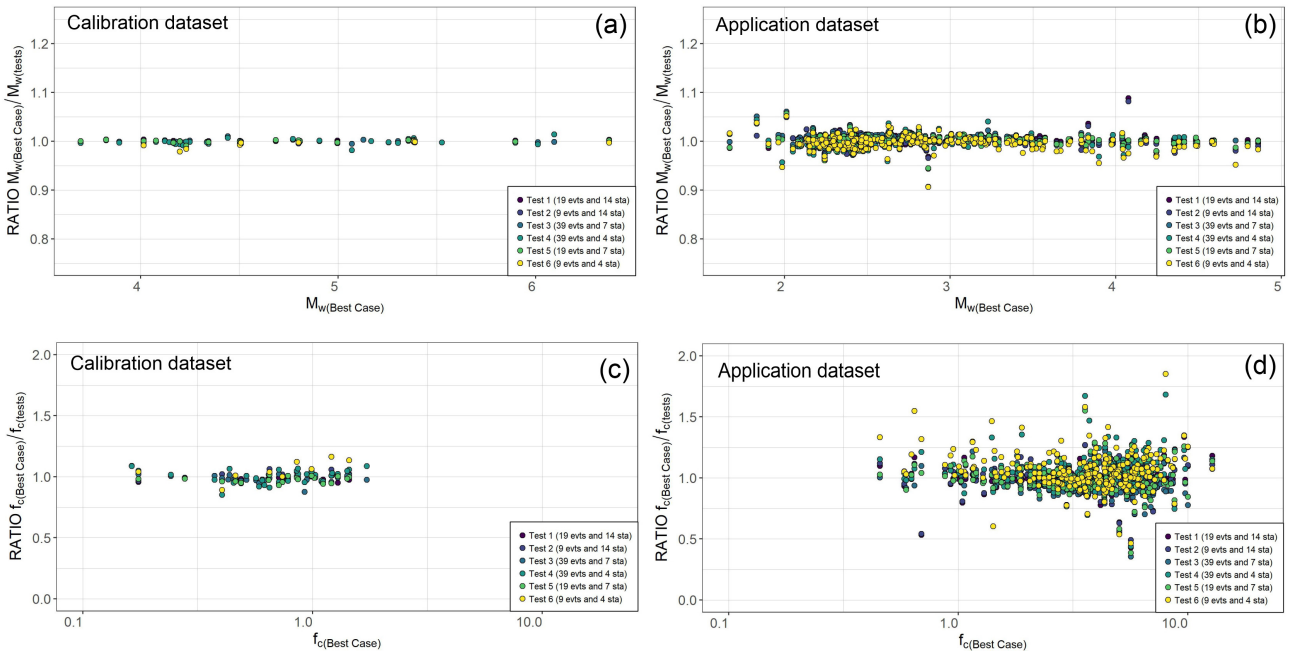

Figure 14. Robustness tests on calibration events (a and c) and application data set (b and d) where we have varied the amount of calibration events and stations to measure how the coda stability might be adversely affected.

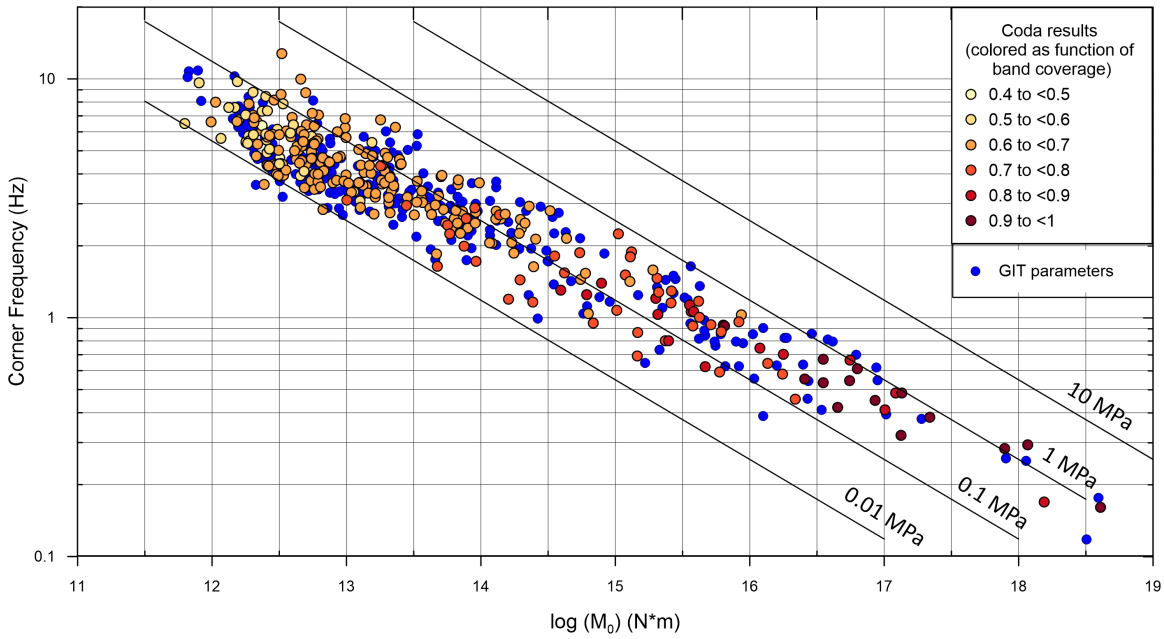

Figure 15. Coda results for the 39 calibration events and for the 247 application events are shown as white to deep red circles as a function of the bandwidth coverage. The colour of the symbols represents the per cent of observed versus observed-plus-model-extrapolated total energy. The higher per cent of observed energy, the lower the uncertainty of the result. Blue circles represent the GIT results for the common events (34 calibration and 247 application events). Lines of constant apparent stress are shown as reference.

247 earthquakes ranging between ∼1.7 to ∼5 were used to evaluate the robustness of the determination of source parameters using the two methodologies.

The robustness of the coda calibration procedure is tested by progressively reducing the number of calibration events and stations and applying each new calibration to the validation data set. In this way, we simulate a calibration in a sparse network region. We observed that even in the case of a reduction of 75 per cent of the number of events and stations with respect to the best case (39 events and 14 stations), M_w and corner frequency estimates remain substantially stable (Fig. 14), and this is true for the application data set.

Since multiple main shock–aftershock sequences occurred in Central Italy in the last several years (Amatrice–Norcia–Visso, 2016–2017; L'Aquila 2009), a large amount of data is available making this region ideal for applying data-driven approaches with the goal of deriving stable source parameters. Thus, to evaluate the performance of the coda calibration approach, we applied another

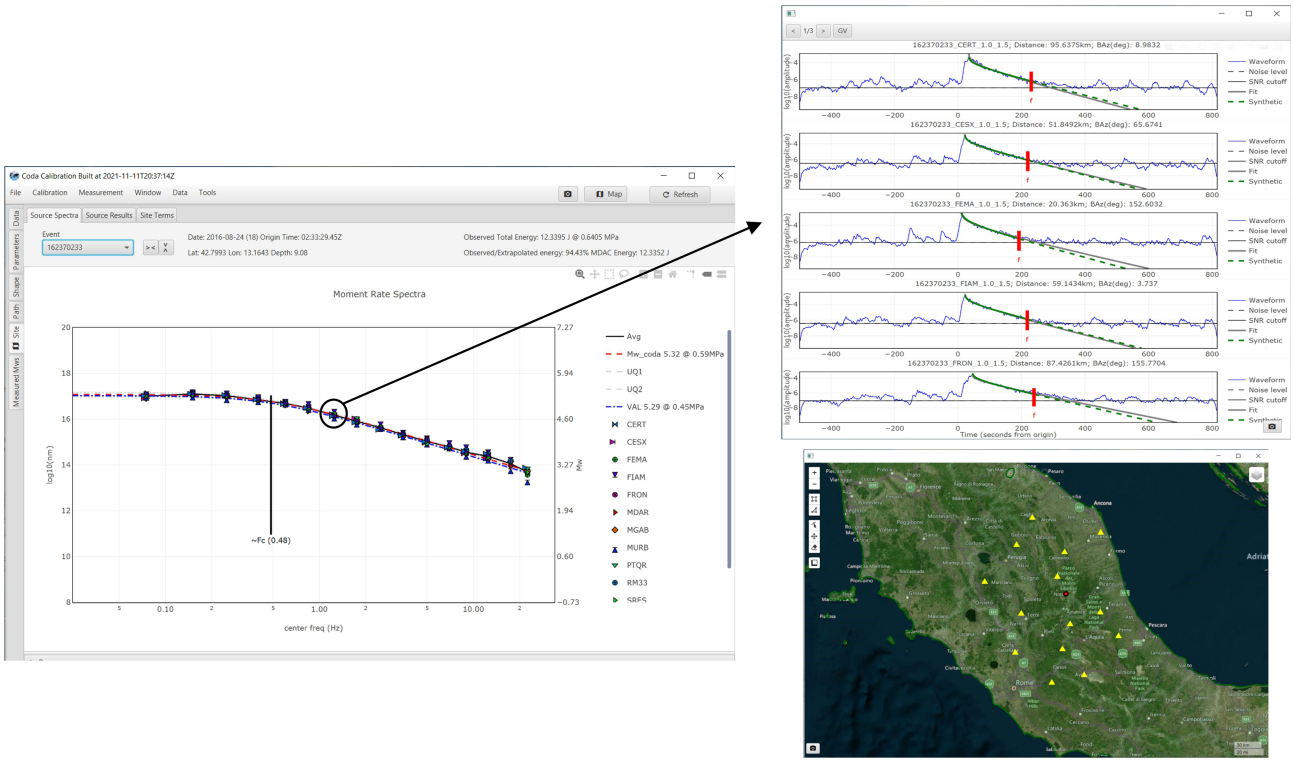

Figure 16. Example source spectra summary page from CCT that can be used in routine automated processing and allows the user to quality check and modify envelope measurements if necessary. The summary page provides source parameter information such as seismic moment, M_w, total radiated energy and apparent stress and provides an interactive map showing the event and stations used.

well-known calibration technique, the GIT (Andrews 1986; Castro *et al.* 1990), a data-driven methodology particularly suitable to this well-sampled region of Italy.

Provided there is ample data, this technique can derive equally stable source parameters because of the high redundancy of information due to the large amount of input data. In fact, the distribution of the GIT-derived apparent source spectra is affected by source radiation pattern, directivity, and complex attenuation phenomena, but if the data set shows high redundancy, the median will be extremely stable. The data set for GIT calibration analysis includes ∼5000 earthquakes and more than 600 stations, comprising 34 of the 39 events used for coda calibration and all the same 14 stations.

As the first step in the validation process, we compared the source spectra derived for the common calibration events and the corresponding source parameters resulted in good agreement (Figs 7 and 8).

For a more significant validation, the two independent sets of calibrated parameters (GIT- and coda-derived) are applied to the validation data set that is composed of events not included in either of the two calibrations. The comparison of the results in terms of source spectra and source parameters (Figs 11 and 12) allows us to confirm the robustness of source parameter estimation, as well as to validate the coda calibration in this region. The consistency of source parameters estimated from analysis performed on different portions of seismic recordings is also a matter of debate for Central Italy (Kemna *et al.* 2021). Figs 11 and 12 show that coda and *S* waves methodologies applied independently to a common data set compiled for central Apennines in Italy provide very similar source spectra, from which consistent scaling laws are extracted.

To have a complete vision of the data analysed in Central Italy using the CCT, Fig. 15 shows the source scaling for all calibration and application events together, along with GIT results for the same events (the source scaling of about 4800 earthquakes used for the GIT spectral decomposition is shown in Fig. S2). Results are comparable to those provided by a recent coda spectral ratio analysis in the same region (Morasca *et al.* 2019) which also showed an increase in apparent stress with increasing magnitude. In that study, the authors analysed the first part of the multiple main shock–aftershock Amatrice–Norcia–Visso sequence, considering events recorded between August and October 2016. They estimated the deviation from self-similarity through the evaluation of the ε parameter following Kanamori & Rivera (2004), obtaining a value of 0.61. Likewise, the study by Malagnini & Munafò (2018) in the same region of Central Italy found a similar increase.

As CCT also provides the observed total radiated energy estimates, including the information on the bandwidth covered for the calculation, the figure shows this information in terms of different colours. All 39 calibration events have at least 70 per cent of bandwidth coverage for the radiated energy estimates, as well as 40 of the application events have the same coverage, including 14 events of $M_w < 3.5$.

We demonstrate that in the seismically active region of Central Italy, the coda calibration method requires a significantly smaller number of calibration events and stations to obtain the same stability in source parameters as the GIT calibration that requires orders of magnitude more events and stations, opening new opportunities to apply this approach for future applications in regions less seismically active and with fewer seismic stations.

It can be applied for a consistent estimation of M_w for small and large events representing an opportunity to improve seismic hazard analysis, critically influenced by this parameter. The events

in the earthquake catalogue used for the seismic hazard assessment must be described according to a unique magnitude scale that should moreover be consistent with the magnitude measure of the ground-motion attenuation relationships used in the seismic hazard calculation.

Typically, conversion relationships from other kinds of magnitudes are applied to small events for which reliable M_w estimations are usually not available, but in some cases a large bias is introduced (e.g. Shelly *et al*. 2021). Once the coda calibration is performed for a region, the application of the obtained parameters to small events within the same region avoids any conversion and provides a stable M_w estimation over a wide range of event sizes.

As the methodology provides robust models, even considering a limited number of events and stations, it could be extended to other regions allowing the homogenization of the M_w estimates for the national territory, maintaining the same level of accuracy also in poorly sampled regions where the application of GIT may not be feasible.

Furthermore, for calibrated regions CCT can be included in routine processing to provide stable source spectra and associated source information for crustal events too small to be waveform modeled. Once new seismic recordings are available that are instrument-corrected and located, CCT can generate the necessary envelopes, estimate the coda measurement windows, apply the calibrated model, and export both measurements and uncertainties automatically. Both the import and export of data use the JavaScript Object Notation (JSON) format. Schema defining the JSON fields and further examples can be found in the Python notebooks in the CCT project on GitHub. Fig. 16, for example, shows a summary source spectra from CCT for an event in Central Italy. The tool allows the user to quality check each measurement data point and make measurement changes to the envelopes if necessary, as well as view the event and associated stations on an interactive map.

Recently, Spallarossa *et al.* (2021) developed a tool for the rapid assessment of source parameters for new earthquakes occurring in Central Italy. The tool is based on empirical models calibrated using GIT analysis on a rich data set; however, to extend the procedure to sparser sampled regions, the coda calibration approach would likely have to be used.

DATA AND RESOURCES

The CCT version 1.0.15 was used in this study and is available from https://github.com/LLNL/coda-calibration-tool/releases/(last accessed January 2022).

The authors used waveform data from the European Integrated Data Archive (EIDA; https://www.orfeus–eu.org/data/eida/, last accessed October 2021). In particular, the authors analysed waveforms recorded by the National Institute of Geophysics and Volcanology (INGV)–Italian National Seismic Network (International Federation of Digital Seismograph Networks [FDSN] code IV, https://doi.org/10.13127/SD/X0FXnH7QfY) and by the RAN–Italian Strong Motion Network (FDSN code IT, https://doi.org/10.7914/SN/IT).

The supplementary material of this paper includes details on the GIT analysis (Figs S1 and S2) and the source spectra of three outliers observed among the calibration events (Fig. S3).

ACKNOWLEDGMENTS

The authors used data from the National Institute of Geophysics and Volcanology (INGV)-Italian national seismic network (International Federation of Digital Seismograph Networks [FDSN] code IV, https://doi.org/10.13127/SD/X0FXnH7QfY) and from the RAN-Italian strong motion network (FDSN code IT, https://doi.org/10.7914/SN/IT). PM was partially supported by the INGV internal project MIUR 2020–2029 ‘Pianeta Dinamico’ – ‘Working Earth: geosciences and understanding of the Earth dynamics and natural hazards’ (CUP D53J19000170001). DB was partially supported by the H2020 European project METIS (grant agreement 945121). KM and JRN were supported by the Air Force Technical Applications Center (AFTAC) at Patrick AFB, Satellite Beach, FL. Work by JB and WRW was performed under the auspices of the U.S. Department of Energy by Lawrence Livermore National Laboratory under Contract DE-AC52-07NA27344.

We would like to thank the Editor Dr Sidao Ni, two anonymous reviewers and Adrien Oth for their comments and suggestions that allowed us to significantly improve the manuscript content and form.

Conflict of Interest

The authors declare that they have no competing interests.

REFERENCES

Abercrombie, R. E, 1995. Earthquake source scaling relationship from 1 to 5 M_L using seismograms recorded at 2.5 km depth, *J. geophys. Res.,* **100,** 24 015–24 036.

Abercrombie, R. E., 2015. Investigating uncertainties in empirical Green’s function analysis of earthquake source parameters, *J. geophys. Res.,* **120,** 4263–4277.

Aki, K., 1969. Analysis of the seismic coda of local earthquakes as scattered waves, *J. geophys. Res.,* **74,** 615–631.

Aki, K., 1980. Attenuation of shear-waves in the lithosphere for frequencies from 0.05 to 25 Hz, *Phys. Earth planet. Inter.,* **21,** 50–60

Aki, K., 1992. Scattering conversions P to S versus S to P, *Bull. seism. Soc. Am.,* **82,** 1969–1972.

Aki, K. & Chouet, B., 1975. Origin of coda waves: source, attenuation and scattering effects, *J. geophys. Res.,* **80,** 3322–3342.

Andrews, D. J., 1986. Objective determination of source parameters and similarity of earthquakes of different size, in *Earthquake Source Mechanics,* pp. 259–267, eds Das, S., Boatwright, J. & Scholz, C. H., American Geophysical Union.

Baltay., A., Prieto, G. & Beroza, G. C., 2010. Radiated seismic energy from coda measurements and no scaling in apparent stress with seismic moment, *J. geophys. Res.,* **115**(B8), doi:10.1029/2009JB006736.

Baltay, A., Ide, S., Prieto, G. & Beroza, G., 2011. Variability in earthquake stress drop and apparent stress. *Geophys. Res. Lett.,* **38**(6). doi:10.1029/2011GL046698.

Baltay, A., Abercrombie, R. E. & Taira, T., 2022. The SCEC/USGS community stress drop validation study using the 2019 Ridgecrest earthquake sequence data, in *Presented at the SSA 2022 Meeting,* Technical Sessions, Seismological Society of America, 19–23 April, Bellevue, Washington, doi:10.1785/0220210025.

Barno, J., 2017. LLNL/coda-calibration-tool, Computer software, https://github.com/LLNL/coda-calibration-tool. USDOE, 19 December 2017, web, doi:10.11578/dc .20180306.1.

Bent, A. L., Mayeda, K., Roman-Nieves, J. I., Shelly, D. & Barno, J., 2022. Coda envelope moment magnitudes and the re-evaluation of magnitude conversion relations for seismic Hazard assessment in southeastern Canada, in *Presented at the 2022 SSA Meeting,* doi: 10.1785/0220220087.

Bindi, D., Spallarossa, D. & Pacor, F., 2017. Between-event and between-station variability observed in the Fourier and response spectra domains: comparison with seismological models, *Geophys. J. Int.,* **210,** 1092–1104.

Bindi, D., Spallarossa, D., Picozzi, M. & Morasca, P., 2020. Reliability of source parameters for small events in central Italy: insights from spectral decomposition analysis applied to both synthetic and real data, *Bull. seism. Soc. Am.,* **110,** 3139–3157

Boatwright, J., Fletcher, J. B. & Fumal, T. E., 1991. A general inversion scheme for source, site and propagation characteristics using multiply recorded sets of moderate-sized earthquakes, *Bull. seism. Soc. Am.,* **81,** 1754–1782.

Bonilla, L. F., Steidl, J. H., Lindley, G. T., Tumarkin, A. G. & Archuleta, R. J., 1997. Site amplification in the San Fernando Valley, California: variability of site-effect estimation using the S-wave, coda, and HIV methods, *Bull. seism. Soc. Am.,* **87,** 710–730.

Brune, J., 1970. Tectonic stress and the spectra from seismic shear waves earthquakes, *J. geophys. Res.,* **75,** 4997–5009.

Brune, J. N., 1971. Correction, *J. geophys. Res.,* **76**(20), 5002.

Campbell, K. W. & Boore, D. M., 2016. Evaluation of six NEHRP B/C crustal amplification models proposed for use in western North America, *Bull. seism. Soc. Am.,* **106,** 673–686.

Castro, R. R., Anderson, J. G. & Singh, S. K., 1990. Site response, attenuation and source spectra of S waves along the Guerrero, Mexico subduction zone, *Bull. seism. Soc. Am.,* **80,** 1481–1503.

CEN. Eurocode 8, 2004. Design of structures for earthquake resistance - part 1: general rules, seismic actions and rules for buildings, European Standard EN 1998-1:20.

Edwards, B., Rietbrock, A., Bommer, J. J. & Baptie, B., 2008. The acquisition of source, path, and site effects from microearthquake recordings using Q tomography: application to the United Kingdom, *Bull. seism. Soc. Am.,* **98,** 1915–1935.

Eken, T., Mayeda, K., Hofstetter, A., Gök, R., Orgulu, G. & Turkelli, N., 2004. An application of the coda methodology for moment-rate spectra using broadband stations in Turkey, *Geophys. Res. Lett.,* **31**(11), doi:10.1029/2004GL019627.

Eshelby, J. D., 1957. The determination of the elastic field of an ellipsoidal inclusion, and related problems, *Proc. R. Soc. A,* **241,** 376–396.

Gök, R. *et al.*, 2016. Moment magnitudes of local/regional events from 1D coda calibrations in the broader Middle East region, *Bull. seism. Soc. Am.,* **106,** 1926–1938.

Holt, J. *et al.*, 2021. Toward robust and routine determination of Mw for small earthquakes: application to the 2020 Mw 5.7 Magna, Utah, seismic sequence, *Seismol. Res. Lett.,* **92**(2A), 725–740.

Hussein, S. *et al.*, 2022. GITEC: a generalized inversion technique benchmark, *Bull. seism. Soc. Am.,* **112**(2), 850–877.

Ide, S. & Beroza, G. C., 2001. Does apparent stress vary with earthquake size?, *Geophys. Res. Lett.,* **28**(17), 3349–3352.

Ide, S., Beroza, G. C., Prejean, S. G. & Ellsworth, W. L., 2003. Apparent break in earthquake scaling due to path and site effects on deep borehole recordings, *J. geophys. Res.,* **108**(B5), 2271.

Kanamori, H., 1977. The energy release in great earthquakes, *J. geophys. Res.,* **82,** 2981–2987.

Kanamori, H. & Rivera, L., 2004. Static and dynamic scaling relations for earthquakes and their implications for rupture speed and stress drop, *Bull. seism. Soc. Am.,* **94**(1), 314–319.

Kato, K., Aki, K. & Takemura, M., 1995. Site amplification from coda waves: validation and application to S-wave site response, *Bull. seism. Soc. Am.,* **85,** 467–477

Keilis-Borok, V. I., 1959. On the estimation of the displacement in an earthquake source and of source dimensions, *Ann. Geofis.,* **12,** 205–214.

Kemna, K. B., Verdecchia, A. & Harrington, R. M., 2021. Spatio-temporal evolution of earthquake static stress drop values in the 2016–2017 central Italy seismic sequence, *J. geophys. Res.,* **126,** e2021JB022566, doi:10.1029/2021JB022566.

Koenker, R. & Ng, P., 2017. SparseM: sparse linear algebra, R package version 1.77, available at: https://CRAN.R-project.org/package = SparseM, last accessed March 2020.

Konno, K. & Ohmachi, T., 1998. Ground-motion characteristics estimated from spectral ratio between horizontal and vertical components of microtremor, *Bull. seism. Soc. Am.,* **88**(1), 228–241.

Madariaga, R., 1976. Dynamics of an expanding circular fault, *Bull. seism. Soc. Am.,* **66,** 639–666

Madariaga, R., 1979. On the relation between seismic moment and stress drop in the presence of stress and strength heterogeneity, *J. geophys. Res.,* **84,** 2243–2250.

Malagnini, L. & Munafò, I., 2018. On the relationship between ML and MW in a broad range: an example from Apennines (Italy), *Bull. seism. Soc. Am.,* **118,** 1018–1024.

Malagnini, L., Akinci, A., Mayeda, K., Munafo, I., Herrmann, R. B. & Mercuri, A., 2011. Characterization of earthquake-induced ground motion from the L'Aquila seismic sequence of 2009, Italy, *Geophys. J. Int.,* **184,** 325–337.

Malagnini, L., Mayeda, K., Nielsen, S., Yoo, S. H., Munafo, I., Rawles, C. & Boschi, E., 2014. Scaling transition in earthquake sources: a possible link between seismic and laboratory measurements, *Pure appl.Geophys.,* **171,** 2685–2707.

Margheriti, L., Wennerberg, L. & Boatwright, J., 1994. A comparison of coda and S-wave spectral ratios estimates of site response in the southern San Francisco bay area, *Bull. seism. Soc. Am.,* **84,** 1815–1830.

Mayeda, K. & Malagnini, L., 2010. Source radiation invariant property of local and near-regional shear-wave coda: application to source scaling for the Mw 5.9 Wells, Nevada sequence, *Geophys. Res. Lett.,* **37**(7), doi:10.1029/2009GL042148.

Mayeda, K. & Walter, W. R., 1996. Moment, energy, stress drop, and source spectra of western United States earthquakes from regional coda envelopes, *J. geophys. Res.,* **101,** 11 195–11 208.

Mayeda, K., Koyanagi, S., Hoshiba, M. & Aki, K., 1992. A comparative study on scattering, intrinsic and coda attenuation in Long Valley, Hawaii, and central California regions, *J. geophys. Res.,* **97,** 6643–6659.

Mayeda, K., Hofstetter, A., O'Boyle, J. L. & Walter, W. R., 2003. Stable and transportable regional magnitudes based on coda-derived moment rate spectra, *Bull. seism. Soc. Am.,* **93,** 224–239.

Mayeda, K., Malagnini, L. & Walter, W. R., 2007. A new spectral ratio method using narrow band coda envelopes: evidence for non-self-similarity in the Hector Mine sequence, *Geophys. Res. Lett.,* **34**. doi:10.1029/2007GL030041.

Murphy, K. R., Mayeda, K. & Walter, W. R., 2009. Coda spectral peaking for Nevada nuclear test site explosions, *Bull. seism. Soc. Am.,* **99,** 441–448.

Morasca, P., Mayeda, K., Malagnini, L. & Walter, W. R., 2005a. Coda derived source spectra, moment magnitudes, and energy-moment scaling in the Western Alps. *Geophys. J. Int.,* **160**(1), 263–275.

Morasca, P., Mayeda, K., Gök, R., Malagnini, L. & Eva, C., 2005b. A break in self-similarity in the Lunigiana-Garfagnana region (Northern Apennines). *Geophys. Res. Lett.,* **32**(22), doi: 10.1029/2005GL024443.

Morasca, P., Walter, W. R., Mayeda, K. & Massa, M., 2019. Evaluation of earthquake stress parameters and its scaling during the 2016 Amatrice sequence, *Geophys. J. Int.,* **218,** 446–455.

Oth, A., Bindi, D., Parolai, S. & Di Giacomo, D., 2011. Spectral analysis of K-NET and KiK-net data in Japan, Part II: on attenuation characteristics, source spectra, and site response of borehole and surface stations, *Bull. seism. Soc. Am.,* **101**(2), 667–687.

Pacor, F. *et al.*, 2016a. Spectral models for ground motion prediction in the L'Aquila region (central Italy): evidence for stress-drop dependence on magnitude and depth, *Geophys. J. Int.,* **204,** 697–718.

Pacor, F., Gallovič, F., Puglia, R., Luzi, L. & D'Amico, M., 2016b. Diminishing high-frequency directivity due to a source effect: empirical evidence from small earthquakes in the Abruzzo region, Italy, *Geophys. Res. Lett.,* **43,** 5000–5008.

Phillips, W. S. & Aki, K., 1986. Site amplification of coda waves from local earthquakes in central California, *Bull. seism. Soc. Am.,* **76,** 627–648.

Picozzi, M., Oth, A., Parolai, S., Bindi, D., De Landro, G. & Amoroso, O., 2017. Accurate estimation of seismic source parameters of induced seismicity by a combined approach of generalized inversion and genetic algorithm: application to The Geysers geothermal area, California, *J. geophys. Res.,* **122,** 3916–3933.

Prejean, S. & Ellsworth, W., 2001. Observations of earthquake source parameters at 2 km depth in the Long Valley caldera, eastern California, *Bull. seism. Soc. Am.,* **91,** 165–177.

Prieto, G. A., Shearer, P. M., Vernon, F. L. & Kilb, D., 2004. Earthquake source scaling and self-similarity estimation from stacking P and S spectra, *J. geophys. Res.,* **109**(B8), doi:10.1029/2004JB003084.

Sato, H. & Fehler, M., 1998. *Seismic Wave Propagation and Scattering in the Heterogeneous Earth: Modern Acoustics and Signal Processing,* AIP Press.

Roman-Nieves, J. I., Mayeda, K. & Soto-Cordero, L., 2021. Towards a local-regional coda source calibration for Puerto Rico: modeling moment-tensors, apparent stress, and scaled energy from the 2019-2020 earthquake sequence, *Seismol. Res. Lett.,* **92**(2A), 725–740.

Shearer, P. M., Abercrombie, R. E., Trugman, D. T. & Wang, W., 2019. Comparing EGF methods for estimating corner frequency and stress drop from P wave spectra, *J. geophys. Res.,* **124**(4), 3966–3986.

Shelly, D. R. *et al.*, 2021. A big problem for small earthquakes: benchmarking routine magnitudes and conversion relationships with coda envelope-derived Mw in Southern Kansas and Northern Oklahoma, *Bull. seism. Soc. Am.,* **112**(1), 210–225.

Singh, S. K. & Ordaz, M., 1994. Seismic energy release in Mexican subduction zone earthquakes, *Bull. seism. Soc. Am.,* **84**(5), 1533–1550.

Spallarossa, D., Picozzi, M., Scafidi, D., Morasca, P., Turino, C. & Bindi, D., 2021. RAMONES, the Rapid Assessment of MOmeNt and Energy Service in Central Italy: concepts, capabilities and future perspectives, *Seismol. Res. Lett.,* **92,** 1759–1772.

Su, F., Anderson, J. G., Brune, J. N. & Zeng, Y., 1996. A comparison of direct S-wave and coda wave site amplification determined from aftershocks of Little Skull Mountain earthquake, *Bull. seism. Soc. Am.,* **86,** 1006–1018.

Trugman, D. T. & Shearer, P. M., 2017. Application of an improved spectral decomposition method to examine earthquake source scaling in Southern California. *J. geophys. Res.,* **122**(4), 2890–2910.

Walter, W. R., Yoo, S.-H., Mayeda, K. & Gök, R., 2017. Earthquake stress via event ratio levels: application to the 2011 and 2016 Oklahoma seismic sequences, *Geophys. Res. Lett.,* **44,** 3147–3155.

Wyss, M. & Brune, J. N., 1968. Seismic moment, stress, and source dimensions for earthquakes in the California-Nevada region, *J. geophys. Res.,* **73**(14), 4681–4694.

Yoo, S.-H. & Mayeda, K., 2013. Validation of non-self-similar source scaling using ground motions from the 2008 Wells, Nevada, earthquake sequence, *Bull. seism. Soc. Am.,* **103,** 2520–2533.

Zeng, Y., 1993. Theory of scattered P- and S-wave energy in a random isotropic scattering medium, *Bull. seism. Soc. Am.,* **83,** 1264–1276.

SUPPORTING INFORMATION

Supplementary data are available at *GJI* online.

Figure S1. Spectral amplitude decomposition results: (a) non-parametric attenuation curves; (b) site amplification curves and (c) non-parametric source curves. In panel (a), coloured lines indicate the attenuation values averaged over frequency intervals selected as indicated in the legend; in panel (b), black lines indicate the amplifications of the three selected reference sites (i.e. stations LSS, RM03 and T1221); in panel (c), black lines show the GIT source spectra of the 2016 Norcia and 2009 L'Aquila main shock earthquakes.

Figure S2. Source parameters of about 4800 earthquakes used for the spectral amplitude decomposition. Top left-hand panel: the seismic moment versus corner frequency scaling is compared to constant stress drop lines (ranging from 0.01 to 10 MPa); symbols are coloured accordingly to logarithm of the radiated energy estimated from the velocity source spectra and corrected for finite-bandwidth effects (Ide & Beroza 2001). Top right-hand panel: apparent stress (right vertical axis) and $\theta k = \log(\mathrm{Er/M0})$ (left vertical axis) versus seismic moment, using $\mu = 30$ GPa. Earthquakes with M_w above 5.5 have an average θk equal to –4.3, in agreement with Kanamori (1977); for smaller magnitudes, the logarithm of the apparent stress scales with the logarithm of seismic moment with an average slope of 0.32. Bottom panel: apparent stress versus Brune (1970, 1971) stress drop considering linear (left-hand side) and logarithmic (right-hand side) scales. On the bottom left-hand panel, the best-fitting line (showin in red) has a slope of 0.2478.

Figure S3. Source spectra for three events with large discrepancy between results from GIT and CCT (red). GIT-derived apparent source spectra are coloured to indicate the different distances (top panel) or azimuth (bottom panel) for the corresponding event–station pair.

Table S0. Independent source information for the 39 calibration events. The four ground-truth (GT) reference events are those with both reference moment magnitude ($M_{\mathrm{w(Ref)}}$) and reference apparent stress ($\sigma_{\mathrm{a(Ref)}}$) in MPa. For two events the independent information is used as validation ($M_{\mathrm{w(Val)}}$ and $\sigma_{\mathrm{a(Val)}}$). For the remaining 33, events we use only reference M_w values ($M_{\mathrm{w(Ref)}}$).

Please note: Oxford University Press is not responsible for the content or functionality of any supporting materials supplied by the authors. Any queries (other than missing material) should be directed to the corresponding author for the paper.